haematologica
Journal of the Ferrata Storti Foundation

Intercellular transfer of FOLR2 from nurse-like cells fuels chronic lymphocytic leukemia cell activation and proliferation

by Marcin Domagala, Chloe Bazile, Bastien Gerby, Loïc Ysebaert, Fabian Coscia, Vera Pancaldi, Camille Laurent and Mary Poupot

Received: May 27, 2026.
Accepted: November 2, 2026.

Citation: Marcin Domagala, Chloe Bazile, Bastien Gerby, Loïc Ysebaert, Fabian Coscia, Vera Pancaldi, Camille Laurent and Mary Poupot. Intercellular transfer of FOLR2 from nurse-like cells fuels chronic lymphocytic leukemia cell activation and proliferation.
Haematologica. 2026 Nov 12. doi: 10.3324/haematol.2026.301318 [Epub ahead of print]

Publisher's Disclaimer.
E-publishing ahead of print is increasingly important for the rapid dissemination of science. Haematologica is, therefore, E-publishing PDF files of an early version of manuscripts that have completed a regular peer review and have been accepted for publication.
E-publishing of this PDF file has been approved by the authors.
After having E-published Ahead of Print, manuscripts will then undergo technical and English editing, typesetting, proof correction and be presented for the authors' final approval, the final version of the manuscript will then appear in a regular issue of the journal.
All legal disclaimers that apply to the journal also pertain to this production process.

Intercellular transfer of FOLR2 from nurse-like cells fuels chronic lymphocytic leukemia cell activation and proliferation

Marcin Domagala[1,2,3*], Chloe Bazile[1,2], Bastien Gerby[1], Loïc Ysebaert[1,4], Fabian Coscia[3], Vera Pancaldi[1,2], Camille Laurent[1,5] and Mary Poupot [1,2*]

[1] University of Toulouse, INSERM, CNRS, CRCT, 31037, Toulouse, France.
[2] Equipe labellisée Ligue Nationale Contre le Cancer.
[3] Max-Delbrück-Center for Molecular Medicine in the Helmholtz Association (MDC), 13125, Berlin, Germany.
[4] Department of Haematology, Institut Universitaire du Cancer de Toulouse - Oncopole, 31059 Toulouse, France.
[5] Service d'anatomopathologie, Institut Universitaire du Cancer de Toulouse - Oncopole, 31059 Toulouse, France.

*Corresponding authors: Mary Poupot (mary.poupot@inserm.fr), 2 avenue Hubert Curien, CRCT (Centre de Recherches en Cancérologie de Toulouse) , CS53717, 31037, Toulouse, France. Phone : +335 82 74 16 62, fax: +335 82 74 16 85; Marcin Domagala (marcinjakub.domagala@mdc-berlin.de), Robert-Rössle-Straße 10, Max-Delbrück-Centrum für Molekulare Medizin in der Helmholtz-Gemeinschaft, 13125, Berlin, Germany. Phone : +49 30 9406-2251.

Contribution: M.D. designed the study, performed the experiments, interpreted data, and wrote the manuscript; C.B. processed the healthy-donor blood samples; B.G. participated in the design of the research; L.Y. provided patients' blood samples and associated clinical data; C.L. provided the patients' lymph node samples, associated clinical data, and supervised IHC staining; V.P. and F.C. provided the funding; M.P provided the funding, designed the study, interpreted data, and wrote the manuscript. All the authors critically reviewed the manuscript.

Authors' disclosures: the authors declare no conflict of interest.

The AI tool ChatGPT (OpenAI) was used solely for post-drafting language editing of text originally written by the authors, including shortening, reformulation, formatting, and grammatical correction to improve clarity and comply with word limits. All AI-assisted text was critically reviewed and revised by the authors, who take full responsibility for the accuracy and integrity of the final manuscript.

Data sharing statement: we can share original data upon request to the corresponding authors.

Acknowledgments: The authors thank all the patients who generously donated clinical samples for this study. This work was supported in part by the Janssen Foundation, Région Midi-Pyrénées, La Ligue Nationale Contre le Cancer, CNRS, and Toulouse III University. We would like to thank the members of the platform IMAG'IN (l'Institut Universitaire du Cancer de Toulouse), especially N. Van Acker, FX. Frenois and A. Belin-Artola for the IHC staining of LN. We are grateful to P. Gravelle for facilitating communication with the Anatomo-Pathology Department of the IUCT Oncopole, and to A. Quillet-Mary for her critical review of the manuscript. Schematics were created using BioRender.com.

ABSTRACT

Communication with the lymphoid microenvironment is essential for the survival and proliferation of neoplastic B cells in chronic lymphocytic leukemia (CLL). While nurse-like cells (NLCs) are recognized as key components of this niche, the mechanisms and functional impact of their interactions with malignant cells remain insufficiently understood. Here, using primary patient cells, we found that NLCs express high levels of folate receptor beta (FOLR2), which correlate with increased survival of leukemic cells *in vitro*. Unexpectedly, we found that CLL cells acquire functional FOLR2 from NLCs via trogocytosis, enhancing their folate uptake. To further study the biological relevance of this phenomenon, we modeled lymphoid microenvironmental activation using CD40L and IL-15, which markedly increased FOLR2 transfer and induced robust NLC-dependent CLL cell activation and proliferation. These processes were closely associated, as FOLR2$^+$ CLL cells represented the predominant population of actively cycling leukemic cells. Under the same conditions, we also observed an additional contact-independent mechanism of FOLR2 transfer, suggesting involvement of extracellular vesicles (EVs). To validate these findings *in situ*, we performed multiplex immunofluorescence analysis of CLL lymph nodes. This confirmed the presence of FOLR2$^+$ NLCs and demonstrated their significant enrichment in more aggressive and proliferative cases. In addition, we detected FOLR2$^+$ CLL cells *in situ*, supporting the occurrence of trogocytosis and possibly EVs mediated-transfer in the lymphoid microenvironment. Together, these results identify FOLR2 as a novel marker of protective NLCs and implicate trogocytosis with NLCs as an important mechanism that enhances CLL cell adaptation and promotes leukemic cell activation and proliferation.

SUMMARY

- CLL cells acquire FOLR2 from NLCs through combination of trogocytosis and contact-independent processes, further associated with leukemic-cell activation and proliferation *in vitro*
- Increased frequency of FOLR2 expressing macrophages in aggressive and proliferative cases of CLL.
- FOLR2 is a marker of M2-like protective NLCs *in vitro*

INTRODUCTION

Chronic lymphocytic leukemia (CLL) is a B cell malignancy, characterized by the clonal accumulation of dysfunctional $CD5^+$ mature-like B cells in the peripheral blood and lymphoid organs, including lymph nodes (LNs)[1]. Peripheral CLL cells are mostly quiescent and migrate to lymphoid organs, where they proliferate through interactions with the specific microenvironment[1]. The CLL microenvironment, which includes T cells, endothelial cells, stromal cells, and nurse-like cells (NLCs)[1,2], is critical for leukemic cell survival and chemoresistance[3–7]. NLCs were first observed in the *in vitro* CLL PBMC cultures [8,9], and described as a monocyte-derived population of M2-like macrophages[10,11] that interact closely with CLL cells, protecting them against spontaneous apoptosis[8,9], and therapeutic and immune attacks[11–13]. NLCs are crucial for attracting leukemic cells to lymphoid organs[1], and their increased numbers in LNs and infiltration into proliferation centers correlate with more aggressive disease[5] and shorter overall survival in patients[5,14].

The supportive impact of NLCs for CLL cells is thought to be mediated through the release of soluble factors[1,2,6,12,15], extracellular vesicles (EVs)[16], and direct cell-cell interactions. Although numerous studies have reported the clustering of CLL cells around NLCs[8,9,17], only a few have characterized the nature and functional impact of these direct interactions with leukemic cells. For instance, vimentin and calreticulin presented by NLCs induce the activation of CLL cells through B-cell receptors, thereby promoting their survival and potential proliferation[2,18]. Moreover, direct contact between NLCs and CLL cells mediated through CD31 on NLCs and CD38/CD100 on CLL cells has been implicated in the proliferation of malignant clones[19]. Furthermore, we showed that trogocytic interaction, partially mediated through CD2/CD58 (LFA-3), is essential for promoting CLL cell survival *in vitro*[20]. Trogocytosis is a peculiar type of direct cell-cell interaction that leads to the rapid acquisition of cellular content, including integral plasma membrane fragments[21]. This mechanism is predominantly unidirectional, enabling recipient cells to acquire new functionalities and modulate immune responses[21–23]. Nevertheless, the full impact of trogocytosis on CLL-NLC communication remains poorly understood and requires further investigation.

The protumoral properties of NLCs are directly linked to their M2-like[11] and immunosuppressive polarization state[24,25], typically defined by high expression of CD68[8,9] and CD163[5,11]. Here, we investigated the functional impact of NLC phenotypes and their interactions with CLL cells. Using primary human blood samples, we showed for the first time that NLCs exhibit elevated levels of folate receptor beta (FOLR2), a myeloid cell-restricted[26] folate transporter[27], which has recently emerged as a specific marker of tumor-associated macrophages[28–30]. Furthermore, we showed that FOLR2 levels on NLCs are strongly associated

with *in vitro* CLL cell survival. Unexpectedly, we discovered that CLL cells acquire functional FOLR2 from NLCs via trogocytosis, with an additional contact-independent component potentially involving EVs, and further defined the link between FOLR2 transfer and increased activation and proliferation of CLL cells. We supported relevance of our *in vitro* results by identifying FOLR2$^+$ NLCs in patient LNs, their association to more aggressive and proliferative disease, and the detection of FOLR2$^+$ leukemic cells *in situ*. We propose FOLR2 as a novel marker of protumoral NLCs, and highlight intercellular material transfer mechanisms like trogocytosis, as a crucial component in CLL-NLC communication, supporting increased adaptation of leukemic cells.

METHODS

Primary human cell isolation and culture

Peripheral blood samples from previously untreated CLL Patients were obtained from the Hematology Department with informed consent and referenced in the INSERM cell bank. According to French law, the INSERM cell bank has been registered with the Ministry of Higher Education and Research (DC-2013-1903) after being approved by an ethics committee (Comité de Protection des Personnes Sud-Ouest et Outremer II). Clinical and Biological annotations of the samples have been reported to the Comité National Informatique et Liberté. Buffy coats from healthy donors (HD) were obtained from Établissement français du sang (EFS, France).

Institutional Review Board Statement: The study was conducted according to the guidelines of the Declaration of Helsinki, and approved by the Institutional Review Board (or Ethics Committee) of INSERM (protocol code DC-2013-1903 and date of approval 2013).

Further details regarding cell isolation, *in vitro* culture conditions, and optimization of heterologous co-culture system, are listed in Supplementary Methods.

Flow cytometry

Cells were stained with titrated antibodies (Supplementary Table S1) and analyzed immediately using LSR II or Fortessa X-20 flow cytometers (BD Pharmingen, France). Data were analyzed with FlowLogic 7.00.2 software (Inivai Technologies). A detailed description of staining protocols and gating strategies is provided in the Supplementary Methods.

FOLR2 gene knockout with RNP Crispr-Cas9

FOLR2 gene knockout (KO) in monocytes used for generation of HD-NLCs was achieved using ribonucleoprotein (RNP)-mediated CRISPR-Cas9 sgRNA method. Three predesigned crRNAs (IDT; sequences listed in Supplementary Table S1) targeting two alleles of FOLR2 gene or negative control sequences were delivered via electroporation Neon Transfection System (Thermo Fisher Scientific). Efficacy of FOLR2 KO was evaluated by qPCR (Fig. S2B) or flow cytometry (Fig. S2D). Further information is provided in Supplementary Methods.

Trogocytosis assay

Autologous NLCs were detached and stained with PKH67 (Sigma) according to the manufacturer's protocol. $PKH67^+$ NLCs were then mixed with purified, naïve CLL cells at a 1:3 ratio in 96-well ultra-low attachment plates (Nunclon Sphera, Thermo Scientific), and incubated at 37°C for 4 h. Subsequently, cells were stained with appropriate antibodies and analyzed by flow cytometry. Purified naïve CLL cells cultured alone were used as a negative control of trogocytosis.

Statistical analysis and results representation

Statistical significance and plotting of the results were performed using Graph Pad Prism 10.1.2 (USA). Statistical tests were selected according to the experimental design, including whether observations were matched or independent, the number of groups, variance assumptions, and the presence of missing values. The statistical test applied for each experiment is indicated in the respective figure legends. Results in the bar plots are presented as mean ± SD. The lines in the middle of the boxes in the box-and-whisker plots represent median values. P values below 0.05 were considered statistically significant.

Figures were edited with Inkscape software. Further information regarding experimental procedures and statistical analyses is listed in Supplementary Methods. Details on key reagents, equipment and software employed in this study are provided in Supplementary Table S1.

RESULTS

FOLR2 expressing NLCs promote survival of CLL cells *in vitro*

The polarization state of TAMs determines their role in the TME[31]. Previously, we showed that M2-like NLCs (CD163^{high}, CD14^{high}, CD209^{pos}, CD64^{low}, and CD86^{low}) interact with and support the survival of CLL cells, unlike M1-like NLCs[10]. To further define the phenotype of protective NLCs, we used CLL PBMC *in vitro* cultures (Fig. 1A) and screened for protein markers associated with protumoral TAMs (Fig. S1A, S1B). This analysis revealed that M2-like NLCs displayed high levels of FOLR2 (Fig. S1A, S1B), further co-detected with CD163, a standard NLC marker[5] (Fig. S1C), and significantly overexpressed (MFI = 23057 vs 4268, n=9, $p<0.003$) compared with M2-like monocyte-derived macrophages (MDMs) (Fig. 1B).

Next, we evaluated the kinetics of FOLR2 expression in CD14^{+} monocytes differentiating into NLCs over 15 days of PBMC culture. FOLR2 signals were detectable in CD14^{+} cells from day 3, peaking on days 9-10 for patient samples P5, P8, and P14 (FOLR2^{+} NLCs), but diminishing drastically toward the end of the culture period for P6, P7, and P21 (FOLR2^{-} NLCs; Fig. 1C, left). Moreover, CLL cell survival exceeded 90% in samples with FOLR2^{+} NLCs but dropped below 75% in those with FOLR2^{-} NLCs (Fig. 1C, right). By systematic analysis of FOLR2 expression by NLCs and CLL survival across 64 patient samples (Fig. 1D-E; more details in Supplementary Table S2), we categorized PBMC cultures into three groups: FOLR2^{high} (MFI>4500, median=16258), FOLR2^{low} (1500<MFI<4500, median=3227) and FOLR2^{neg} (MFI<1500, median=340). CLL cell viability varied significantly among these groups (Fig.1E), being highest in the FOLR2^{high} group (mean=94.2%, n=40) and lowest in the FOLR2^{neg} group (mean=57.5%, n=14). Furthermore, leukemic cell viability was significantly higher in PBMC than in purified CLL cell cultures only in samples from the FOLR2^{high} group (Fig. S1D). Finally, among the analyzed myeloid markers on NLCs, the expression of FOLR2 showed the strongest correlation with the viability of CLL cells (Fig. 1F, S1E), followed by that of CD163 and CD14. In contrast, M1 markers CD64 and CD86 were negatively associated with cancer cell survival.

These results indicate that FOLR2 is a specific marker of protective M2-like NLCs that support CLL cell survival *in vitro*.

FOLR2 is detected on CLL cells co-cultured with NLCs

Given that CLL cells drive the maturation of FOLR2^{+} NLCs, which in turn protect leukemic cells from apoptosis[14,32], we explored the potential connection between FOLR2 and the interactions between these two cell types.

During standard phenotyping of NLCs, we observed a subpopulation of lymphoid cells with variable surface expression of the myeloid markers CD14, CD163, CD206 and FOLR2 (Fig. 2A; Fig. S2A for gating strategy), of which only FOLR2 was significantly detected (Fig.2B). Further analyses confirmed that

FOLR2 was absent on freshly isolated $CD5^+/CD19^+$ CLL cells and appeared only after long-term PBMC culture (Fig. 2C), despite the lack of *FOLR2 gene* expression in leukemic cells (Fig. S2B). These results suggested that CLL cells acquire FOLR2 from other cells present in PBMC cultures, most likely NLCs.

To verify this hypothesis, we performed *FOLR2* knockout (KO) experiments in NLCs. To generate a sufficient number of NLCs for KO experiments, we used a healthy donor NLC (HD-NLC) system, in which HD-MDMs were co-cultured with purified CLL cells (Fig. 2D). HD-NLCs correspond to NLCs in terms of functionality[9] and comparable FOLR2 expression (Fig. S2C). Before initiating co-cultures with CLL cells, the efficiency of *FOLR2* knockout in HD-MDMs was verified by flow cytometry (Fig. S2D). Co-cultures with *FOLR2*-KO HD-NLCs led to a significant decrease in the percentage of $FOLR2^+$ CLL cells compared to the control condition (Fig. 2E), confirming that NLCs are the source of FOLR2 detected on CLL cells.

CLL cells acquire functional FOLR2 from NLCs via trogocytosis

As CLL cells engage in trogocytosis with NLCs[20], we investigated whether this mechanism was responsible for FOLR2 acquisition by leukemic cells. First, we co-cultured purified CLL cells with PKH67 stained NLCs for 4h, and measured PKH67 and myeloid marker levels in leukemic cells by flow cytometry (Fig. 3A left). Across 15 measurements, a mean of 20% and 2% of CLL cells were positive for PKH67 and FOLR2, respectively, while the signals from CD14 and CD16 were absent (Fig. 3A right). Next, using confocal microscopy, we demonstrated the direct interaction between $FOLR2^+$ NLCs and $CD19^+$ CLL cells (Fig. 3B left), and observed characteristic FOLR2 positive patches (Fig. 3B right) co-localizing with the plasma membranes of leukemic cells (Fig. S3A). This signal was absent in in co-cultures with *FOLR2*-KO HD-NLCs (Fig. S3B). Physical separation of CLL cells from HD-NLCs by Transwell inserts for 24 or 72h also prevented detectable FOLR2 acquisition by CLL cells (Fig. 3C) and decreased CLL cells viability (Fig. S3C). Furthermore, cytochalasin D significantly reduced FOLR2 acquisition, whereas GW4869 treatment promoted pronounced clustering of CLL cells around HD-NLCs (Fig. S3D) and significant increase of FOLR2 acquisition after 24h (Fig. 3D). Collectively, these results indicate that CLL cells acquire FOLR2 via trogocytosis and that this protein transfer is at least partially selective.

To test whether the FOLR2 acquired by CLL cells was functional, we incubated the co-cultures with EC17, a folic acid-FITC imaging agent[33] . As expected, $FOLR2^+$ NLCs showed higher intracellular EC17 signals than FOLR2 KO NLCs (Fig. 3E). As for $CD19^+$ CLL cells, we observed some with FOLR2 positive membrane patches and intracellular EC17 signal (Fig. 3E, top), which was greatly reduced in FOLR2 KO condition (Fig. 3E, bottom). Moreover, only CLL cells purified after co-culture with HD-NLCs, but not *FOLR2*-KO HD-NLCs, were

positive for EC17 (Fig. 3F). Finally, flow cytometry revealed an increased signal from the folic acid fluorescent probe in the subpopulation of FOLR2^{high} CLL cells compared to FOLR2^{neg} CLL cells (Fig. S3E). The data indicate that FOLR2 acquired via trogocytosis is functional and facilitates folate uptake by CLL cells.

Trogocytic FOLR2^{+} CLL cells are predominantly activated C

Next, we tested whether FOLR2 acquisition by CLL cells was linked to their activation and proliferation. Considering that *in vivo*, CLL cells can engage in trogocytosis only in the presence of the TME, which is further required for their proliferation, we aimed to optimize the culture conditions to mimic the LN microenvironment. To generate macrophage numbers comparable to those in lymphoid organs, we used the HD-NLC co-culture system and substituted other cellular components of the TME with soluble factors (Fig. S4A).

First, we compared IL-2+CpG[34] and CD40L[1]+IL-15[34–36] stimulation to induce distinct activation programs. We selected CD40L+IL-15 treatment, which induced NLC-dependent CLL cell activation, reflected by CD23[37] upregulation and CD184[38] downregulation (Fig. S4B_1), and concomitantly increased the frequency of FOLR2^{+} CLL cells (Fig. S4B_2). Next, we determined that an initial macrophage-to-leukemic-cell ratio of 1:9 most efficiently supported FOLR2 acquisition by CLL cells (Fig. S4C). We finalized the activation protocol by adding cytokines and changing the medium to minimize nutrient depletion (Fig. 4A).

Using the optimized protocol, we confirmed significantly increased CLL cell survival in co-cultures with HD-NLCs compared to monoculture (Fig. S4D). Moreover, we observed increased expression of the positive activation markers CD23, CD49d[39,40], and CD58[18,42] and decreased expression of the negative activation marker CD184 in CLL cells co-cultured with HD-NLCs compared to monocultures (Fig. 4B; Fig. S4E for gating strategy). Next, we demonstrated a significantly higher proportion of FOLR2^{+} CLL cells upon CD40L+IL-15 activation (9 vs 40%; Fig. 4C), which further led to detection of myeloid markers CD11b and CD14 on leukemic cells (Fig. S4F), and strong grouping of the CLL cells around HD-NLCs (Fig.S4H).

We next examined whether physical separation of CLL cells from macrophages affected FOLR2 acquisition under these activation conditions. In contrast to the marked inhibition observed in the absence of external activation (Fig. 3C), CD40L+IL-15-stimulated CLL cells displayed moderate FOLR2 acquisition after 72h despite using a Transwell system (Fig. 4D, S4I). This indicates that, under strong activation conditions, contact-independent mechanisms additionally contribute to FOLR2 transfer.

Subsequently, we compared the activation status of FOLR2^{-} and FOLR2^{+} CLL cells and observed a higher proportion of FOLR2^{+} cells in the CD23^{+}, CD49d^{+}, CD58^{+}, and CD184^{low} subpopulations of leukemic cells

(Fig. 4E). We further supported these findings by demonstrating a significant correlation between the FOLR2 enrichment score (ES_{FORL2}; Fig. S4G) and the total percentage of CLL cells expressing the corresponding activation marker (Fig. 4F).

Taken together, these results demonstrate that CD40L+IL-15 treatment induces strong NLC-dependent activation of leukemic cells, greatly promotes the acquisition of FOLR2 by CLL cells, and that $FOLR2^+$ CLL cells are predominantly activated.

$FOLR2^+$ CLL cells are the predominant subpopulation of proliferating leukemic cells

Next, we explored whether transfer of FOLR2-containing membranes from NLCs supports CLL cell proliferation.

We first assessed the effects of HD-NLCs and CD40L+IL-15 stimulation on Ki67 expression in CLL cells. While neither co-culture with HD-NLCs nor CD40L+IL-15 stimulation alone substantially affected CLL cell proliferation (Fig. S5A), their combination induced robust Ki67 expression in CLL cells (Fig. 5A; gating strategy shown in Fig. S5B). Since Ki67 marks actively cycling cells[43], we performed a CellTrace™ Violet (CTV) dye-dilution assay to quantify the cumulative fraction of cells undergoing division. This analysis further confirmed that co-culture with HD-NLCs, combined with CD40L+IL-15 stimulation significantly enhanced CLL cell proliferation (Fig. S5C).

We next examined the relationship between FOLR2 levels and the proliferation status of CLL cells. We detected the majority of $Ki67^+$ CLL cells in the activated $CD23^+/CD184^{low}$ and $FOLR2^+$ subpopulations of leukemic cells (Fig.5B). By calculating a Ki67 enrichment score (ES_{Ki67}; Fig. S4G), representing the proportion of $Ki67^+$ events within the $FOLR2^+$ cell fraction, we found a strong correlation between ES_{Ki67} and total percentage of $Ki67^+$ CLL cells (Fig. 5C), demonstrating $FOLR2^+$ CLL cell enrichment in the fraction of actively proliferating cells.

Subsequently, we investigated the impact of folic acid (FA) availability on CLL cell proliferation and FOLR2 acquisition. We first assessed the effect of FA deprivation on proliferation under three culture conditions with decreasing FA content: FA^{high} (>1000 µg/L), FA^{low} (~1.22 µg/L), and $FA^{negative}$ (~0 µg/L), using patient samples previously characterized by high proliferative capacity. Reduction of FA limited CLL cell proliferation in a dose-dependent manner, as evidenced by significantly decreased Ki67 expression (Fig. 5D, top) and reduced CTV dilution (Fig. 5D, bottom). Moreover, depletion of FA led to significantly smaller

frequency of FOLR2$^+$ CLL cells and decreased proportion of FOLR2 levels on CLL cells (Fig. S5D). Next, we studied the distribution of FOLR2$^+$ CLL cells in the subpopulation of actively cycling cells, depending on the FA availability (Fig. 5E). By combining Ki67 and CTV staining, we defined four subpopulations of CLL cells: P1 (CTV^{high}Ki67$^-$) – quiescent cells; P2 (CTV^{high}Ki67$^+$) – cells right before the first division; P3 (CTV^{low}Ki67$^+$) – actively cycling cells after the first division; P4(CTV^{low}Ki67$^-$) – quiescent cells after previous proliferation (Fig. 5E). Analysis of FOLR2 levels in each subpopulation of CLL cells revealed dynamic fluctuations, with low levels in non-activated cells before the first division (P1), a significant increase in actively proliferating cells (P2, P3), and a significant decrease in cells that had ceased proliferating (P4; Fig. S5E), regardless of the initial FA content. Finally, we observed stable FOLR2 levels in the subsequent generations of actively proliferating CLL cells (Fig. 5F)

These experiments demonstrated enrichment of FOLR2$^+$ CLL cells within the fraction of actively cycling leukemic cells, revealing a close association between FOLR2 acquisition and NLC-dependent CLL cell proliferation.

Detection of FOLR2$^+$ leukemic cells in the lymph nodes of CLL patients

Finally, we studied FOLR2 expression in tissues from CLL patients (Supplementary Table S3) to validate some aspects of our *in vitro* findings. Using multiplex immunofluorescence (mIF), we measured FOLR2 and CD163 expression by macrophages in the reactive tonsil (n=1) from a healthy donor, and in LNs from patients with CLL, including cases ranging from classical CLL (cCLL; n=5), to accelerated CLL (aCLL; n=10) and CLL with Richter transformation (RT-CLL; n=5). We observed an increasing number of CD163$^+$ macrophages expressing FOLR2 between reactive tonsils and CLL subtypes with increasing aggressiveness (Fig. 6A), and demonstrated a significantly higher proportion of FOLR2 expressing CD163$^+$ macrophages (MΦ) in aCLL and RT-CLL than in cCLL cases (Fig. 6B). Although not statistically significant, the analysis showed a trend toward a higher frequency of FOLR2$^+$ NLCs in aCLL and RT-CLL cases (Fig.S6A).

Moreover, we detected CD20$^+$ leukemic cells containing FOLR2 patches co-localizing with both the plasma membrane and cell interior (Fig. 6C, Fig. S6B), indicating FOLR2 transfer occurrence to leukemic cells, as previously demonstrated *in vitro*. Next, we investigated the potential relationship between FOLR2$^+$ MΦ and cancer cell proliferation. We observed that FOLR2$^+$ MΦ were closely associated with Ki67$^+$ leukemic cells (Fig. 6D). Using global image quantification (n = 17), we stratified the patient samples into

groups with low (<25% Ki67$^+$) and high (>25% Ki67$^+$) cancer cell proliferation (Fig. 6E), and found that the infiltration of FOLR2$^+$ MΦ was significantly more elevated in the high-proliferation group.

Taken together, these findings confirm the presence of FOLR2$^+$ MΦ in patient LNs and demonstrate an association between a higher proportion of FOLR2-expressing MΦ and more aggressive and proliferative CLL cases. In addition, the detection of FOLR2$^+$ leukemic cells provides in situ evidence of intercellular FOLR2 transfer from macrophages to leukemic cells.

DISCUSSION

Previously, we showed that the M2-like polarization state of NLCs[10] and their direct interactions with CLL cells, including trogocytosis[20], are essential for preventing spontaneous apoptosis of leukemic cells *in vitro*. Here, we identified FOLR2 as a novel marker of protective NLCs. Moreover, we demonstrated that CLL cells acquire the functional FOLR2 from NLCs via trogocytosis and potentially EVs, which is associated with increased activation and proliferation of leukemic cells. Finally, we observed an elevated proportion of FOLR2 expressing macrophages in the patient LNs from aggressive subtypes of CLL, that also correlates with leukemic cell proliferation, and we detected FOLR2$^+$ leukemic cells *in situ,* collectively supporting the relevance of intercellular material transfer in CLL pathophysiology.

A key finding of our study is the discovery of rapid trogocytic transfer of functional FOLR2 from NLCs to CLL cells, revealing a direct mechanistic link between FOLR2$^+$ NLCs and the enhanced activation and proliferation of leukemic cells. Owing to its high affinity and rapid turnover[26,41,42], FOLR2 gives trogocytic CLL cells an advantage in folate uptake, molecules essential for one-carbon metabolism, cell growth and proliferation. This may explain why FOLR2$^+$ CLL cells are a predominant subpopulation of activated and proliferating leukemic cells in co-cultures with NLCs, particularly in conditions with limited access to folic acid. Moreover, we demonstrated that the actively cycling population of CLL cells maintain a stable level of extracellular FOLR2, which declines once proliferation ceases, further linking FOLR2 acquisition with observed *in vitro* phenotype. These findings are supported by our observation that CLL cells remain in close contact with FOLR2$^+$ macrophages in CLL LNs, the association between the overall infiltration of FOLR2$^+$ NLCs and more proliferative disease, and the detection of FOLR2$^+$ leukemic cells *in situ*. In the literature, we can find similar examples of trogocytosis contributing to increased cell adaptability. For instance, Lu et al. demonstrated that NK-cells can acquire the tyrosine kinase receptor TYRO3 from tumor cells, resulting in increased NK-cell activation and proliferation[43]. Similarly, colon cancer

cells use trogocytosis to acquire lymphocyte-derived CD4, CD45, CTLA4 and Tim3, thereby promoting their immunosuppressive capabilities[23].

Our data indicate an unexplored bias in protein transfer during CLL-NLC interactions. Among the tested proteins, FOLR2 was the main NLC-derived protein detectable in CLL cells under resting conditions. Unlike the integral transmembrane proteins CD16, CD163, and CD206[44], FOLR2 is a small GPI-anchored membrane protein, suggesting that trogocytosis primarily involves the outer leaflet of the NLC plasma membrane. Although CD14 is also a small GPI-anchored protein co-expressed with FOLR2, its transfer and retention on CLL cells were markedly lower, further highlighting the selectivity of FOLR2 acquisition. Moreover, upon CD40L+IL-15 priming, we observed not only an increase in the transfer of FOLR2 to leukemic cells but also the acquisition of CD11b and CD14, indicating that activation intensifies the interaction between CLL cells and NLCs, and the trogocytosis process itself. Given that FOLR2 reportedly inhibits CD11b/CD18-mediated macrophage adhesion[45] and decreased adhesion promotes trogocytosis in macrophages[46], we suggest that FOLR2 could modulate CLL–NLC contact dynamics, which could explain its preferential acquisition by CLL cells.

Besides trogocytosis, our data confirmed contribution of contact-independent mechanisms in the transfer of FOLR2 from NLCs to CLL cells. While physical separation of CLL cells from NLCs with Transwell inserts abolished the FOLR2 transfer in the resting conditions, it led to partial acquisition of this protein upon CD40L+IL-15 stimulation, suggesting transfer by EVs. Indeed, induction of EV-release upon cell activation has been demonstrated before[47], while work by Ikhlef et al. reported that NLCs produce EVs with pro-survival impact on CLL cells[16]. However, treatment with the EV release inhibitor GW4869 did not reduce FOLR2 transfer and was instead associated with increased FOLR2 acquisition and enhanced clustering of CLL cells around NLCs. These findings argue against EVs being the predominant mechanism of FOLR2 transfer and further support the importance of direct cell-cell interactions, particularly trogocytosis, in this process.

While we demonstrated a clear association between FOLR2 expression and the protective phenotype of NLCs, the exact role of FOLR2 in the functionality of these cells remains to be explored. In macrophages, FOLR2 expression has been proposed to promote folate accumulation and stabilization of an immunosuppressive phenotype through epigenetic changes[27]. This aligns with findings that NLCs are immunosuppressive and promote T-helper cell expansion, thereby weakening antitumor immunity [25]. We further speculate that FOLR2^{high} NLCs might act as folate reservoirs for proliferating CLL cells, particularly during phases of rapid disease expansion when systemic folate availability becomes limiting [27].

Although FOLR2 acquisition partially explains the phenotype of trogocytic CLL cells, additional molecules transferred from NLCs likely contribute to their enhanced activation and proliferation. Trogocytosis could potentially support CLL cells via transfer of activating receptors, or by facilitating cross-presentation of autoantigens[48] from NLCs. Moreover, trogocytosis with NLCs could help CLL cells optimize their metabolic requirements by mediating acquisition of lipids and other biomolecules required for cell proliferation[21,49].

This study highlights the central role of FOLR2$^+$ NLCs in supporting CLL cells, and characterizes a novel trogocytosis-mediated pro-tumoral interaction between these two cell types. We believe that uncovering the intricacies of intercellular material transfer in CLL, including trogocytosis, could increase our understanding of cancer cell interactions within the TME, leading to more efficient therapeutic strategies, with relevance for other types of cancers.

References

1. Kipps TJ, Stevenson FK, Wu CJ, et al. Chronic lymphocytic leukaemia. Nat Rev Dis Primers. 2017;3:17008.
2. Koehrer S, Burger JA. Chronic lymphocytic leukemia: disease biology. Acta Haematol. 2024;147(1):8-21.
3. Lagneaux L, Delforge A, Bron D, De Bruyn C, Stryckmans P. Chronic lymphocytic leukemic B cells but not normal B cells are rescued from apoptosis by contact with normal bone marrow stromal cells. Blood. 1998;91(7):2387-2396.
4. Burger JA, Quiroga MP, Hartmann E, et al. High-level expression of the T-cell chemokines CCL3 and CCL4 by chronic lymphocytic leukemia B cells in nurselike cell cocultures and after BCR stimulation. Blood. 2009;113(13):3050-3058.
5. Boissard F, Laurent C, Ramsay AG, et al. Nurse-like cells impact on disease progression in chronic lymphocytic leukemia. Blood Cancer J. 2016;6(1):e381.
6. Zaaboub R, Vimeux L, Contremoulins V, et al. Nurselike cells sequester B cells in disorganized lymph nodes in chronic lymphocytic leukemia via alternative production of CCL21. Blood Adv. 2022;6(16):4691-4704.
7. Guo Y, Pei H, Lu B, et al. Aberrantly expressed Wnt5a in nurse-like cells drives resistance to Venetoclax in chronic lymphocytic leukemia. Cell Death Discov. 2022;8(1):82.
8. Burger JA, Tsukada N, Burger M, Zvaifler NJ, Dell'Aquila M, Kipps TJ. Blood-derived nurse-like cells protect chronic lymphocytic leukemia B cells from spontaneous apoptosis through stromal cell-derived factor-1. Blood. 2000;96(8):2655-2663.
9. Tsukada N, Burger JA, Zvaifler NJ, Kipps TJ. Distinctive features of "nurselike" cells that differentiate in the context of chronic lymphocytic leukemia. Blood. 2002;99(3):1030-1037.
10. Domagala M, Ysebaert L, Ligat L, et al. IL-10 rescues CLL survival through repolarization of inflammatory nurse-like cells. Cancers (Basel). 2022;14(1):16.
11. Ysebaert L, Fournié JJ. Genomic and phenotypic characterization of nurse-like cells that promote drug resistance in chronic lymphocytic leukemia. Leuk Lymphoma. 2011;52(7):1404-1406.
12. Chen Y, Chen L, Yu J, et al. Cirmtuzumab blocks Wnt5a/ROR1 stimulation of NF-kB to repress autocrine STAT3 activation in chronic lymphocytic leukemia. Blood. 2019;134(13):1084-1094.
13. Boissard F, Fournié JJ, Quillet-Mary A, Ysebaert L, Poupot M. Nurse-like cells mediate ibrutinib resistance in chronic lymphocytic leukemia patients. Blood Cancer J. 2015;5:e355.
14. Jia L, Clear A, Liu FT, et al. Extracellular HMGB1 promotes differentiation of nurse-like cells in chronic lymphocytic leukemia. Blood. 2014;123(11):1709-1719.
15. Talbot H, Saada S, Barthout E, et al. BDNF belongs to the nurse-like cell secretome and supports survival of B chronic lymphocytic leukemia cells. Sci Rep. 2020;10(1):12572.
16. Ikhlef L, Ratti N, Durand S, et al. Extracellular vesicles from type-2 macrophages increase the survival of chronic lymphocytic leukemia cells ex vivo. Cancer Gene Ther. 2024;31(8):1164-1176.
17. Niemann CU, Herman SEM, Maric I, et al. Disruption of in vivo chronic lymphocytic leukemia tumor-microenvironment interactions by ibrutinib: findings from an investigator-initiated phase II study. Clin Cancer Res. 2016;22(7):1572-1582.
18. ten Hacken E, Gounari M, Back JW, et al. Calreticulin as a novel B-cell receptor antigen in chronic lymphocytic leukemia. Haematologica. 2017;102(10):e394-e396.
19. Deaglio S, Vaisitti T, Bergui L, et al. CD38 and CD100 lead a network of surface receptors relaying positive signals for B-CLL growth and survival. Blood. 2005;105(8):3042-3050.
20. Boissard F, Tosolini M, Ligat L, et al. Nurse-like cells promote CLL survival through LFA-3/CD2 interactions. Oncotarget. 2017;8(32):52225-52236.

21. Joly E, Hudrisier D. What is trogocytosis and what is its purpose? Nat Immunol. 2003;4(9):815.
22. Schriek P, Ching AC, Moily NS, et al. Marginal zone B cells acquire dendritic cell functions by trogocytosis. Science. 2022;375(6581):eabf7470.
23. Shin JH, Jeong J, Maher SE, Lee HW, Lim J, Bothwell ALM. Colon cancer cells acquire immune regulatory molecules from tumor-infiltrating lymphocytes by trogocytosis. Proc Natl Acad Sci U S A. 2021;118(48):e2110241118.
24. Giannoni P, Pietra G, Travaini G, et al. Chronic lymphocytic leukemia nurse-like cells express hepatocyte growth factor receptor (c-MET) and indoleamine 2,3-dioxygenase and display features of immunosuppressive type 2 skewed macrophages. Haematologica. 2014;99(6):1078-1087.
25. Vaca AM, Ioannou N, Sivina M, et al. Activation and expansion of T-follicular helper cells in chronic lymphocytic leukemia nurselike cell co-cultures. Leukemia. 2022;36(5):1324-1335.
26. Samaniego R, Domínguez-Soto Á, Ratnam M, et al. Folate receptor β (FRβ) expression in tissue-resident and tumor-associated macrophages associates with and depends on the expression of PU.1. Cells. 2020;9(6):1445.
27. Samaniego R, Palacios BS, Domínguez-Soto Á, et al. Macrophage uptake and accumulation of folates are polarization-dependent in vitro and in vivo and are regulated by activin A. J Leukoc Biol. 2014;95(5):797-808.
28. Cresswell GM, Wang B, Kischuk EM, et al. Folate receptor beta designates immunosuppressive tumor-associated myeloid cells that can be reprogrammed with folate-targeted drugs. Cancer Res. 2021;81(3):671-684.
29. Xia W, Hilgenbrink AR, Matteson EL, Lockwood MB, Cheng JX, Low PS. A functional folate receptor is induced during macrophage activation and can be used to target drugs to activated macrophages. Blood. 2009;113(2):438-446.
30. Zhang F, Huang B, Utturkar SM, et al. Tumor-specific activation of folate receptor beta enables reprogramming of immune cells in the tumor microenvironment. Front Immunol. 2024;15:1354735.
31. Bied M, Ho WW, Ginhoux F, Blériot C. Roles of macrophages in tumor development: a spatiotemporal perspective. Cell Mol Immunol. 2023;20(9):983-992.
32. Boissard F, Fournié JJ, Laurent C, Poupot M, Ysebaert L. Nurse like cells: chronic lymphocytic leukemia associated macrophages. Leuk Lymphoma. 2015;56(5):1570-1572.
33. De Jesus E, Keating JJ, Kularatne SA, et al. Comparison of folate receptor targeted optical contrast agents for intraoperative molecular imaging. Int J Mol Imaging. 2015;2015:469047.
34. Schleiss C, Ilias W, Tahar O, et al. BCR-associated factors driving chronic lymphocytic leukemia cells proliferation ex vivo. Sci Rep. 2019;9(1):701.
35. De Totero D, Meazza R, Capaia M, et al. The opposite effects of IL-15 and IL-21 on CLL B cells correlate with differential activation of the JAK/STAT and ERK1/2 pathways. Blood. 2008;111(2):517-524.
36. Gupta R, Li W, Yan XJ, et al. Mechanism for IL-15-driven B cell chronic lymphocytic leukemia cycling: roles for AKT and STAT5 in modulating cyclin D2 and DNA damage response proteins. J Immunol. 2019;202(10):2924-2944.
37. Takács F, Tolnai-Kriston C, Hernádfői M, et al. The effect of CD86 expression on the proliferation and the survival of CLL cells. Pathol Oncol Res. 2019;25(2):647-652.
38. Pozzo F, Forestieri G, Vit F, et al. Early reappearance of intraclonal proliferative subpopulations in ibrutinib-resistant chronic lymphocytic leukemia. Leukemia. 2024;38(8):1712-1721.
39. Bulian P, Shanafelt TD, Fegan C, et al. CD49d is the strongest flow cytometry-based predictor of overall survival in chronic lymphocytic leukemia. J Clin Oncol. 2014;32(9):897-904.
40. Burger M, Hartmann T, Krome M, et al. Small peptide inhibitors of the CXCR4 chemokine receptor (CD184) antagonize the activation, migration, and antiapoptotic responses of CXCL12 in chronic lymphocytic leukemia B cells. Blood. 2005;106(5):1824-1830.
41. Puig-Kröger A, Sierra-Filardi E, Domínguez-Soto A, et al. Folate receptor β is expressed by tumor-associated macrophages and constitutes a marker for M2 anti-inflammatory/regulatory macrophages. Cancer Res. 2009;69(24):9395-9403.

42. Gutiérrez-Seijo A, García-Martínez E, Barrio-Alonso C, et al. Activin a sustains the metastatic phenotype of tumor-associated macrophages and is a prognostic marker in human cutaneous melanoma. J Invest Dermatol. 2022;142(3 Pt A):653-661.e2.
43. Lu T, Ma R, Li Z, et al. Hijacking TYRO3 from tumor cells via trogocytosis enhances NK-cell effector functions and proliferation. Cancer Immunol Res. 2021;9(10):1229-1241.
44. Yu S, Guo Z, Johnson C, Gu G, Wu Q. Recent progress in synthetic and biological studies of GPI anchors and GPI-anchored proteins. Curr Opin Chem Biol. 2013;17(6):1006-1013.
45. Machacek C, Supper V, Leksa V, et al. Folate receptor β regulates integrin CD11b/CD18 adhesion of a macrophage subset to collagen. J Immunol. 2016;197(6):2229-2238.
46. Rollins KR, Fiaz S, Datta I, Morrissey MA. Target cell adhesion limits macrophage phagocytosis and promotes trogocytosis. J Cell Biol. 2025;224(11):e202502034.
47. Essandoh K, Yang L, Wang X, et al. Blockade of exosome generation with GW4869 dampens the sepsis-induced inflammation and cardiac dysfunction. Biochim Biophys Acta. 2015;1852(11):2362-2371.
48. Miyake K, Karasuyama H. The role of trogocytosis in the modulation of immune cell functions. Cells. 2021;10(5):1255.
49. Ogier C, Solomon AMC, Lu Z, et al. Trogocytosis of cancer-associated fibroblasts promotes pancreatic cancer growth and immune suppression via phospholipid scramblase anoctamin 6 (ANO6). bioRxiv. 2023 Sep 17. doi: 10.1101/2023.09.15.557802. [preprint, not peer-reviewed].

Figures Legends

Figure 1. FOLR2 is a marker of protective NLCs. A) Schematic representation of NLC generation by high-density CLL PBMC cultures *in vitro*. **B)** Comparison of FOLR2 expression among different types of *in vitro* generated macrophages: NLCs, M2-like, and M1-like monocyte-derived macrophages (MDMs). **Left:** representative flow cytometry histograms; **right**: summary of results from n = 9 independent experiments, each using macrophages from a different CLL patient or healthy donor samples. Statistical significance was assessed using Kruskal–Wallis test followed by Dunn's multiple-comparisons test. **C)** Left: flow cytometric measurement of FOLR2 expression by $CD14^+$ cells during monocyte-to-NLC differentiation over 15 days of CLL PBMC culture, for patients P5-8, P14 and P21. FOLR2 expression is presented as the MFI ratio of anti-FOLR2 staining to the corresponding isotype control; each dot represents an individual measurement. Right: Annexin V/7-AAD dot plots of CLL cells from the same patients, measured on day 12 of PBMC culture. **D-E)** FOLR2 expression by NLCs and CLL cell viability were analyzed in PBMC cultures from n = 64 patient samples on days 12–14 (Supplementary Table 2 for details). **D)** Samples were stratified according to FOLR2 expression by NLCs into three groups: $FOLR2^{neg}$ (MFI < 1500, median = 340, n = 14); $FOLR2^{low}$ (1500 < MFI < 4500, median = 3227, n = 10); $FOLR2^{high}$ (MFI>4500, median = 16258; CLL viability >85%; n = 40). **E)** Comparison of CLL cell viability among groups defined by FOLR2 expression by NLCs. Statistical significance was assessed using Welch's one-way ANOVA followed by Dunnett's T3 multiple-comparisons test. **F)** Association between CLL cell survival and myeloid marker expression by NLCs. Based on CLL cell viability measured between days 12-14, samples were stratified into three ordered survival categories: low (<70%), intermediate (70-85%), and high (>85%) survival. Associations between NLC marker expression and the ordered CLL cell survival categories were assessed using Spearman rank correlation. The lower triangular of the matrix shows Spearman's correlation coefficients (ρ) values between tested parameters, according to color coded scale; the upper triangular of the matrix displays corresponding P values. Results from n = 58 different patient samples. P values < 0.05 were considered statistically significant.

Figure 2. Detection of FOLR2 on the surface of CLL cells. All experimental data shown in panels **A–C** and **E** were obtained by flow cytometry. **A)** Representative dot plots of FOLR2, CD14, CD163, and CD206 expression on cells from CLL PBMC cultures on days 12-14. Upper panels: large, granular cells corresponding to NLCs; lower panels: small cells corresponding to lymphoid cells. **B)** Quantification of the lymphoid-cell populations shown in panel A, expressed as the percentage of cells positive for FOLR2, CD14, CD163, or CD206. Results from n = 19 patient samples. Statistical significance was assessed using a mixed-

effects model (REML) with matching across markers, followed by Tukey's multiple-comparisons test. **C)** FOLR2 expression on purified $CD5^+CD19^+$ CLL cells immediately after isolation from blood (day 0) or after 12 days of PBMC culture. **D)** Schematic representation of FOLR2 knockout (KO) generation in NLCs using a ribonucleoprotein (RNP) CRISPR–Cas9 approach co-culture system comprising healthy donor (HD) $CD14^+$ monocytes and purified CLL cells. **E)** Effect of FOLR2 KO in NLCs on FOLR2 detection on $CD5^+CD19^+$ CLL cells in heterologous co-cultures. **Left:** exemplary dot plots showing FOLR2 expression on CLL cells after co-culture with control (CTRL) HD-NLCs or *FOLR2* KO HD-NLCs. **Right:** combined percentage of $FOLR2^+$ CLL cells after co-culture with CTRL HD-NLCs or *FOLR2* KO HD-NLCs. Results from n = 5 independent experiments using CLL cells from 4 patients and monocytes from 6 healthy donors, comprising 12 unique CLL patient–healthy donor combinations in total. Results were compared using the Wilcoxon matched-pairs signed-rank test. P values <0.05 were considered statistically significant.

Figure 3. CLL cells acquire functional FOLR2 from NLCs via contact-dependent membrane transfer. A) Flow cytometric measurements of PKH67, FOLR2, CD14, and CD16 acquisitions by CLL cells after 4 hours of co-culture with $PKH67^+$ NLCs. **Left:** representative dot plots. **Right:** combined results from n = 3 independent experiments using cells from 5 patients (15 measurements for PKH67 and FOLR2, 7 for CD14, and 8 for CD16). Statistical comparison of the percentages of CLL cells positive for FOLR2, CD14, and CD16 was performed using mixed-effect model, followed by Tukey multiple-comparisons test. **B)** Confocal microscopy images of CLL–NLC co-cultures stained with anti-CD19 (cyan) and anti-FOLR2 (red) antibodies. Left: cell–cell contact between NLCs and CLL cells, represented as 3D projection. Right: detection of FOLR2 patches on the plasma membrane pf CLL cells following interaction with NLCs. **C–D)** Flow cytometric analysis of FOLR2 transfer from macrophages to CLL cells following physical (C) or pharmacological (D) interference with intercellular transfer. Results from n = 3 independent experiments using 5 different patient samples. C) Percentage of $FOLR2^+$ CLL cells after 24 or 72h of co-culture in transwell system. CC - control co-culture without transwell insert; CA - CLL cells cultured alone; TSW_MDM and TSW_NLC – CLL cells cultured in the lower compartment and physically separated by a transwell membrane from MDMs or NLCs, respectively. D) FOLR2 acquisition by CLL cells after 24 h of co-culture with NLCs in the presence of cytochalasin D (CytoD) or GW4869. FOLR2 levels were normalized to the corresponding DMSO-treated direct co-culture control. Results were analyzed using a mixed-effects model, with matching across conditions, followed by Dunnett's multiple-comparisons test versus CC control. P values <0.05 were considered statistically significant. **E)** Confocal microscopy of CLL co-cultures with control (CTRL) HD-NLCs

(upper) or *FOLR2* KO HD-NLCs (lower), incubated with folic acid–FITC (green) for 90 min; images represented as 3D projections. **F)** Epifluorescent images of purified CLL cells after co-culture with CTRL HD-NLCs (upper) or FOLR2 KO HD-NLCs (lower), followed by 90min incubation with folic acid–FITC.

Figure 4. FOLR2 acquisition by CLL cells is positively associated with their activation. All experimental data shown in panels **B–F** were obtained by flow cytometry. **A)** Optimized heterologous co-culture system used to study the relationship between NLC–CLL cell interactions, FOLR2 acquisition, and CLL cell activation. **B)** Representative histograms showing expression of the activation markers CD23, CD58, CD49d, and CD184, together with FOLR2, on CD40L+IL-15-activated CLL cells cultured alone (white) or with HD-NLCs (green). **C)** Percentage of $FOLR2^+$ CLL cells in HD-NLC co-cultures following CD40L+IL-15 activation. Statistical significance was assessed using analyzed using paired, two-tailed Wilcoxon test. **D)** Effect of physical separation from macrophages on FOLR2 acquisition by activated CLL cells. $FOLR2^+$ CLL cells were quantified 24 h and 72 h after activation in direct CLL–HD-NLC co-cultures (CC), CLL cells cultured alone (CA), or transwell co-cultures in which CLL cells were physically separated from MDMs (TSW_MDM) or HD-NLCs (TSW_NLC). Results are shown as the percentage of $FOLR2^+$ CLL cells (left graph for each time point) and after normalization to the corresponding direct co-culture control (right graph). Results were analyzed using a mixed-effects model, with matching across conditions, followed by Dunnett's multiple-comparisons test versus CC control. **E)** Representative dot plots showing co-expression of FOLR2 with CD23, CD58, CD49d, and CD184 on CLL cells following co-culture with HD-NLCs and CD40L+IL-15 activation. **F)** Pearson correlations between the total percentage of CLL cells expressing CD23, CD58, or CD49d, or displaying low CD184 expression, and the corresponding FOLR2 enrichment score (ES_FOLR2), representing the proportion of $FOLR2^+$ cells within the respective activated CLL cell population. Results from n = 5 independent experiments using samples from 12 patients (150 measurement points). P values <0.05 were considered statistically significant.

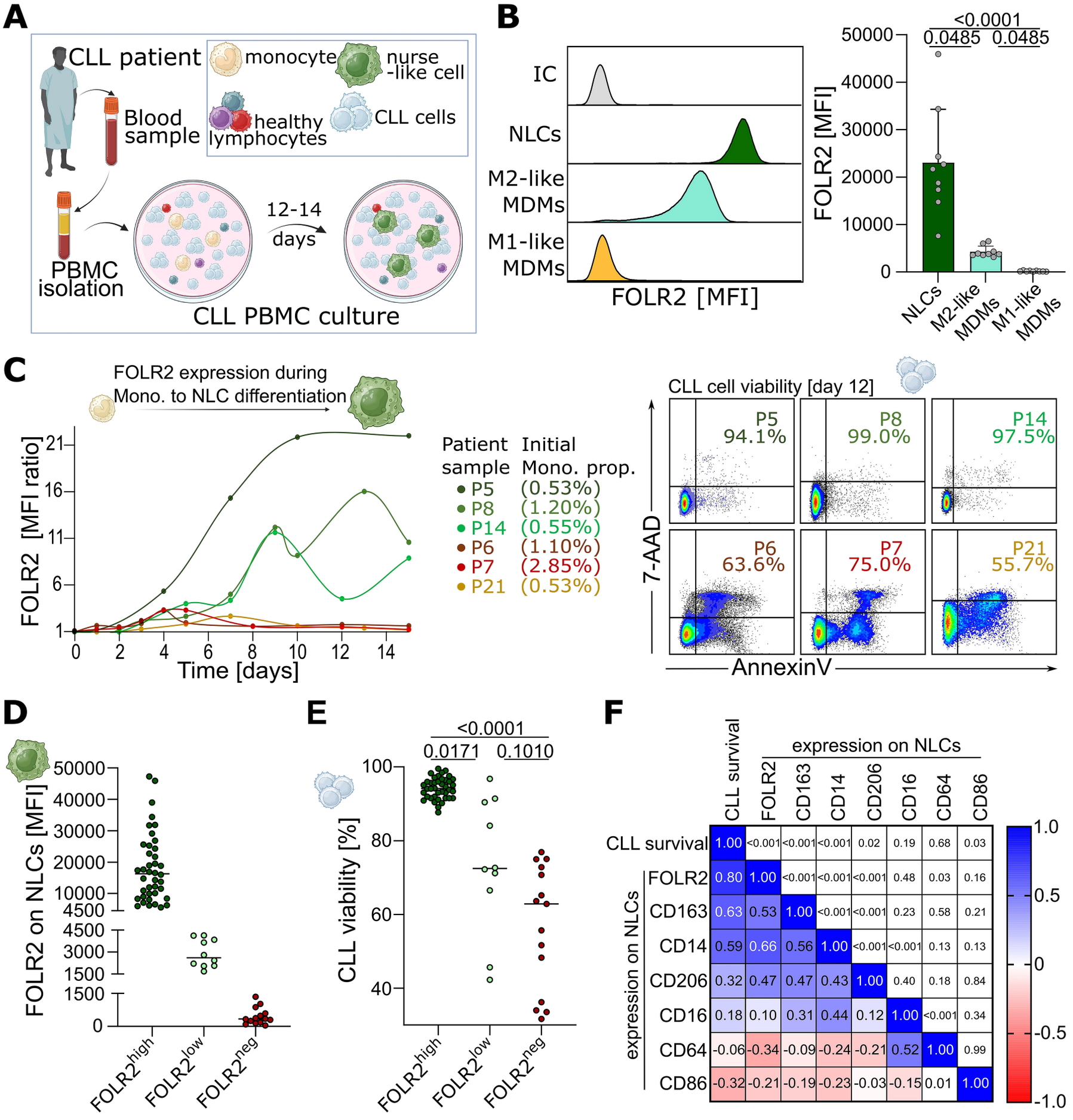
Figure 5. Proliferating leukemic cells are enriched within the population of FOLR2+ CLL cells. All measurements were performed by flow cytometry. **A)** CLL cells were cultured alone or co-cultured with HD-NLCs and activated with CD40L and IL-15. The percentage of $Ki67^+$ CLL cells was compared between the two culture conditions using the Wilcoxon matched-pairs signed-rank test (n = 3 independent experiments; samples from 12 patients; 17 paired measurements). **B)** Representative dot plots showing Ki67, CD23, CD184, and FOLR2 expression in CLL cells activated with CD40L and IL-15, and cultured either alone or with HD-NLCs. **C)** Pearson correlation between the total fraction of $Ki67^+$ CLL cells and the Ki67

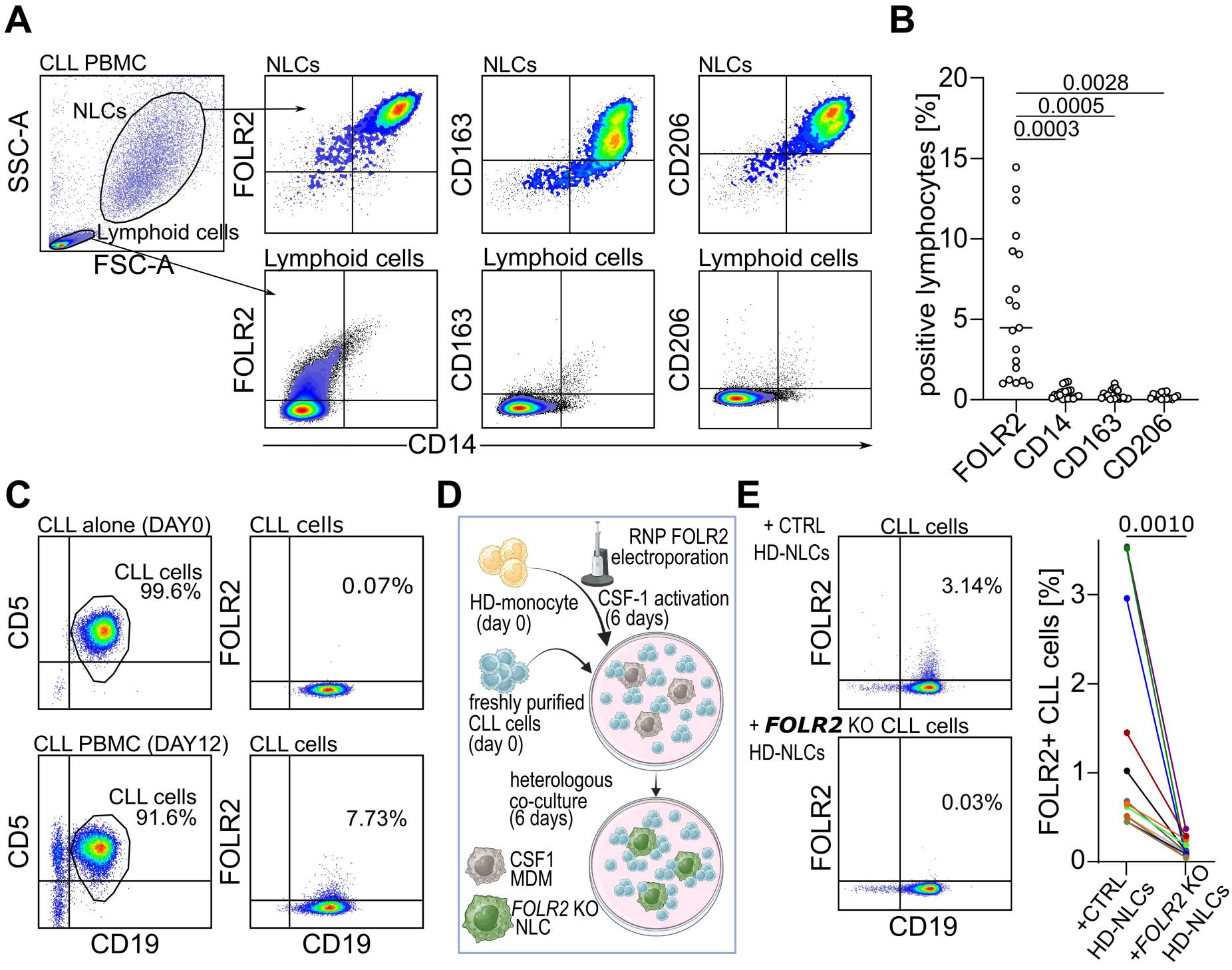
enrichment score (ES_{ki67}, Fig. S4F_B), representing the proportion of $Ki67^+$ cells within the $FOLR2^+$ trogocytic population of leukemic cells. Results from n = 5 independent experiments; samples from 12 patients; 150 measurement points. **D)** Percentage of actively cycling CLL cells ($Ki67^+$, top) and total fraction of CLL cells after cells division, identified by CTV dilution (CTV^{low}, bottom), after co-culture with HD-NLCs and activation with CD40L and IL-15, under the indicated folate conditions. Results from n = 6 different patient samples. Statistical significance was assessed using repeated-measures one-way ANOVA with Geisser–Greenhouse correction, followed by Tukey's multiple-comparisons test. **E)** Analysis of CD23, CD184, and FOLR2 signals on CLL cells gated based on Ki67/CTV levels: P1 = $CTV^{high}/Ki67^-$ (quiescent, non-dividing); P2 = $CTV^{high}/Ki67^+$ (right before first division); P3 = $CTV^{low}/Ki67^+$ (actively cycling, after division); P4 = $CTV^{low}/Ki67^-$ (post-cycling, quiescent). **F)** Exemplary stacked histograms of FOLR2 expression in CLL cells according to proliferative status defined by Ki67/CTV and number of cell generations (G1–G5). FOLR2 expression is shown as median fluorescence intensity (MFI). Results with P values < 0.05 were considered statistically significant.

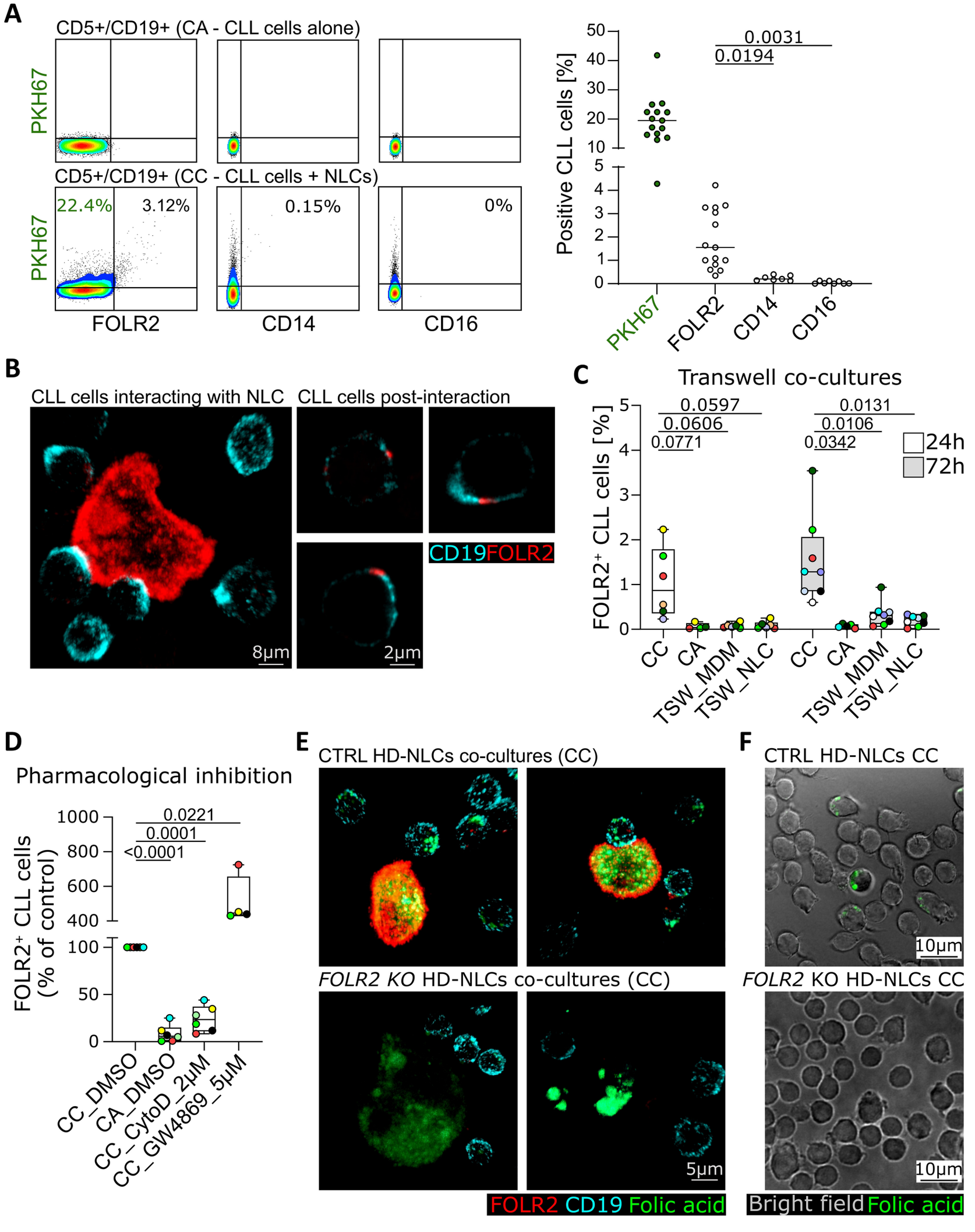
Figure 6. Detection of FOLR2 expression in the lymph nodes of CLL patients. Multiplex immunofluorescence of lymph nodes (LNs) from n = 20 CLL patients (patient characteristic available in Supplementary table S3). Whole FFPE 4µm tissue sections were stained with anti-CD20 (cyan), anti-FOLR2 (yellow), anti-CD163 (purple/green), anti-Ki67 (red; expect #176-178) antibodies, counterstained with DAPI (blue), and visualized with an Axioscan microscope (A, E; 20x) or a Zeiss 980 confocal microscope (C, D; Plan-Apochromat, 40x, 1.3 Oil; 3D-projection of 20 z-stacks/0.5µm).

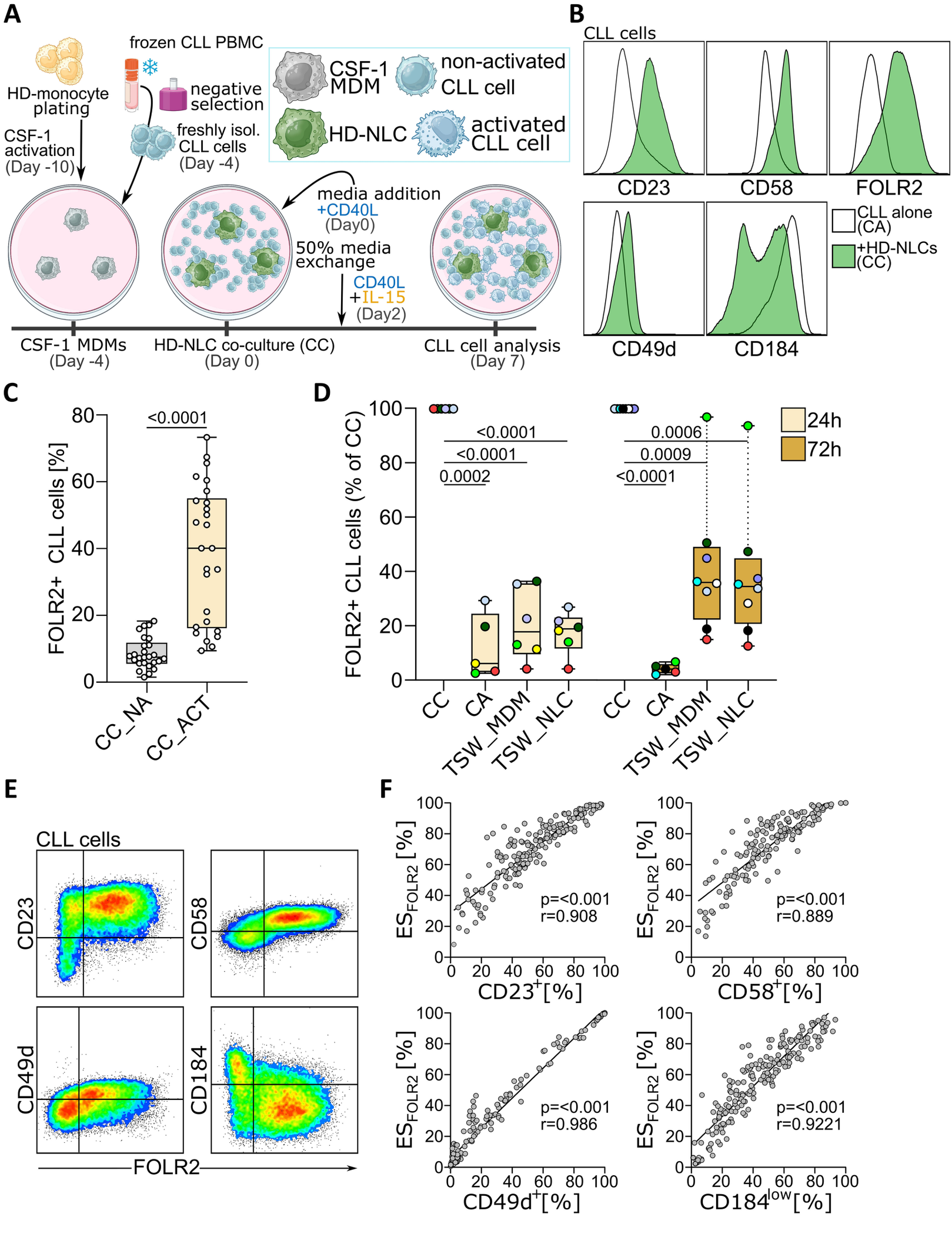
A) Representative images of a reactive tonsil from healthy donor (n = 1), and patients with classical CLL (#191), accelerated CLL (#183), and CLL with Richter Transformation (RT, #193). Top: large-field images; bottom: magnified regions highlighting a variable level of FOLR2 expression on $CD163^+$ macrophages (MΦ). **B)** Comparison of the proportion of FOLR2 expressing cells among $CD163^+$ MΦ in samples from patients with classical CLL (n = 5), accelerated CLL (n = 10), or CLL with RT (n = 5). Statistical significance was analyzed using Kruskal–Wallis test followed by Dunn's multiple-comparisons test. **C)** Detection of FOLR2 signal patches in the plasma membrane (white arrows) or within $CD20^+$ leukemic cells (patients #190, #183, and #193). Dashed lines indicate regions visualized by full-thickness XZ and XY orthogonal projections. **D)** Detection of $FOLR2^+CD163^+$ MΦ in proximity to $Ki67^+$ leukemic cells. **E) Left:** overview images showing $FOLR2^+$ MΦ in relation to $Ki67^+$ leukemic cells in patients with low (#187) and high (#193) cancer cell proliferation. **Right:** the proportion of $FOLR2^+$ MΦ and proliferating $Ki67^+CD20^+$ leukemic cells were quantified across the whole tissue region. Based on the percentage of $Ki67^+$ leukemic cells, samples were

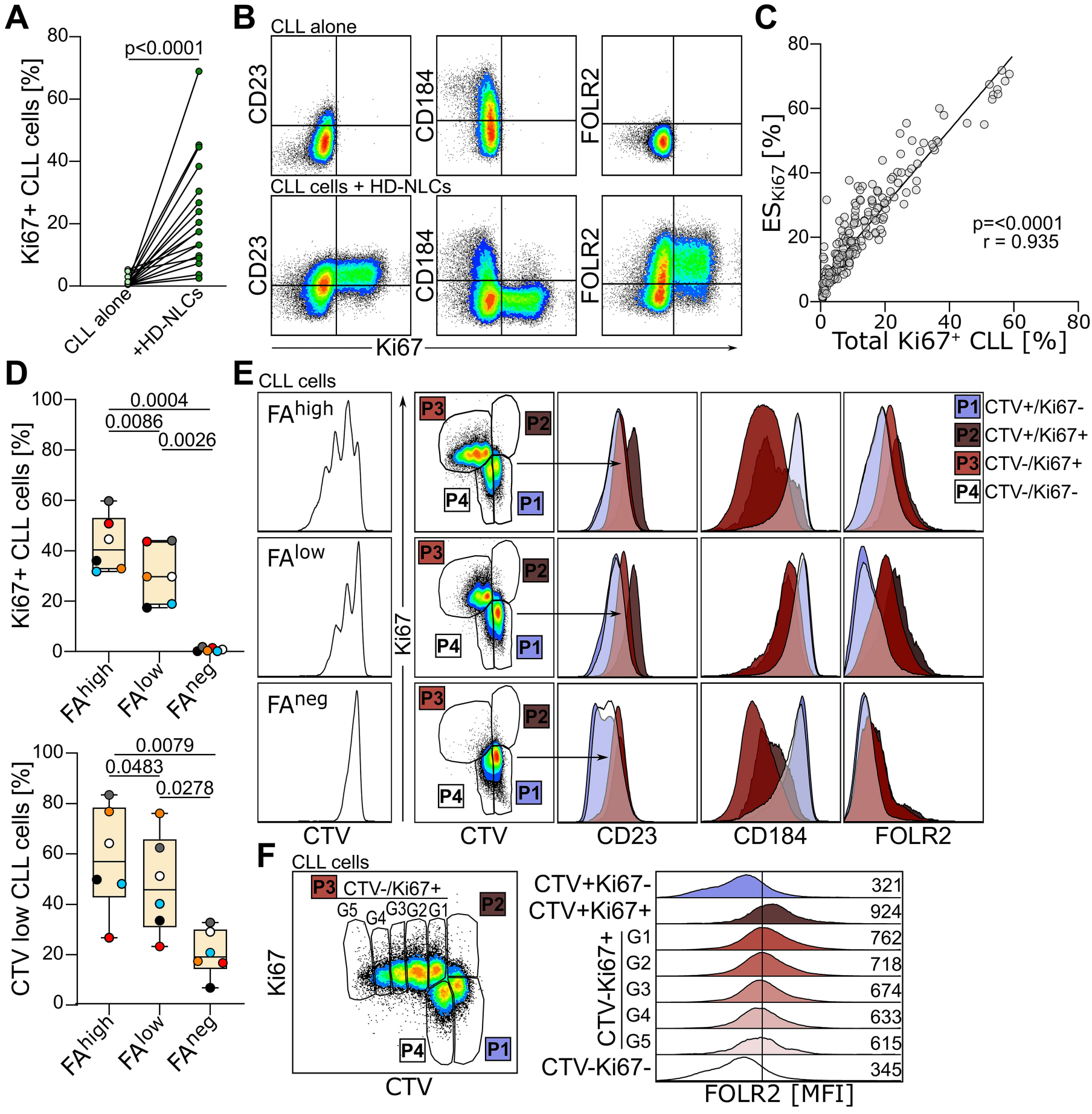
categorized using the cohort median (25%) into low-proliferation (<25%; n = 8) and high-proliferation (>25%; n = 9) groups. The proportion of $FOLR2^+$ macrophages was compared between groups using the Mann–Whitney U-test. P values < 0.05 were considered statistically significant.

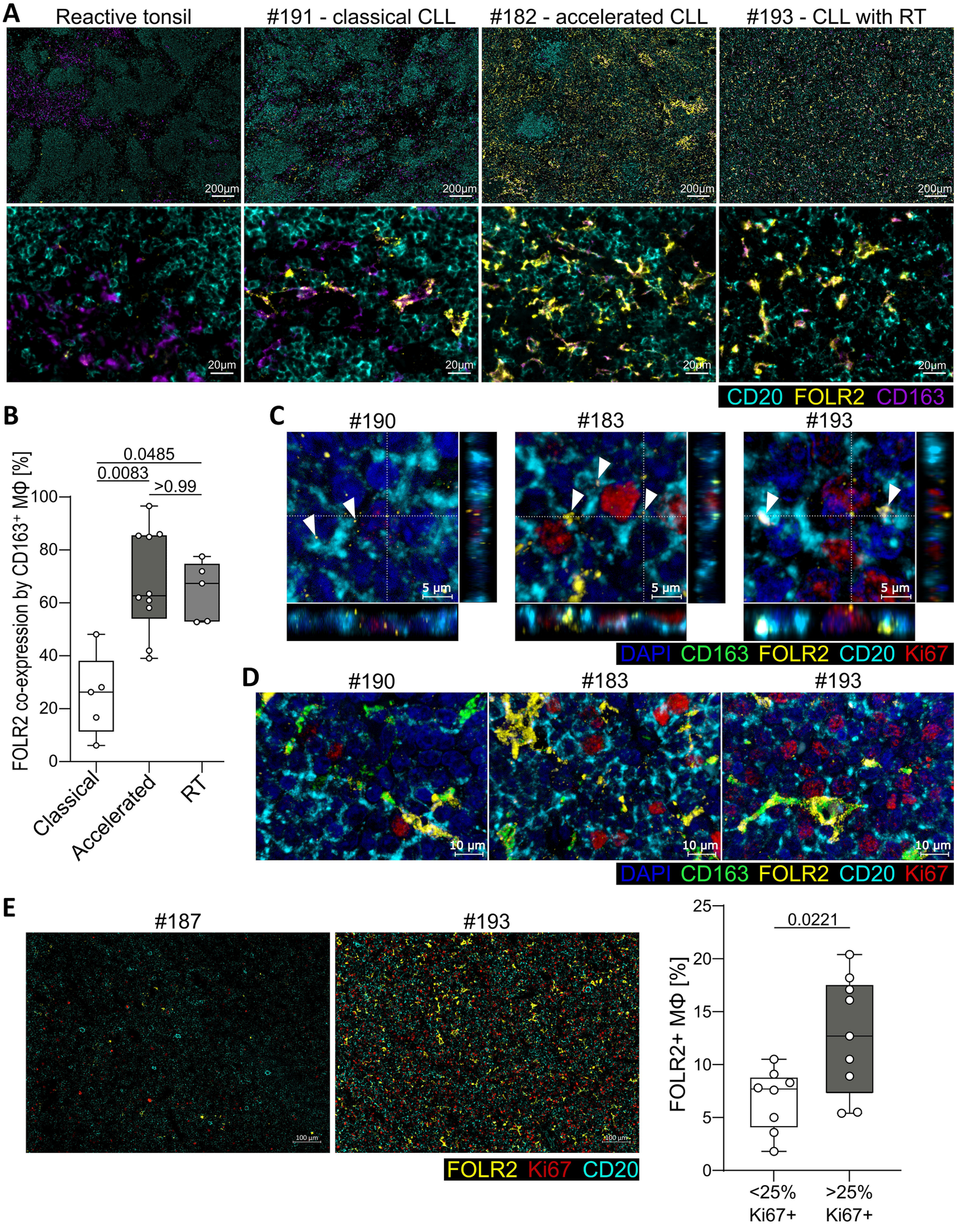

A
CLL patient
Blood sample
PBMC isolation
monocyte
nurse -like cell
healthy lymphocytes
CLL cells
12-14 days
CLL PBMC culture
B
IC
NLCs
M2-like MDMs
M1-like MDMs
FOLR2 [MFI]
<0.0001
0.0485
0.0485
FOLR2 [MFI]
NLCs
M2-like MDMs
M1-like MDMs
C
FOLR2 expression during Mono. to NLC differentiation
FOLR2 [MFI ratio]
Time [days]
Patient sample
Initial Mono. prop.
P5 (0.53%)
P8 (1.20%)
P14 (0.55%)
P6 (1.10%)
P7 (2.85%)
P21 (0.53%)
CLL cell viability [day 12]
P5 94.1%
P8 99.0%
P14 97.5%
P6 63.6%
P7 75.0%
P21 55.7%
7-AAD
AnnexinV
D
FOLR2 on NLCs [MFI]
FOLR2high
FOLR2low
FOLR2neg
E
<0.0001
0.0171
0.1010
CLL viability [%]
FOLR2high
FOLR2low
FOLR2neg
F
CLL survival
expression on NLCs
FOLR2
CD163
CD14
CD206
CD16
CD64
CD86
CLL survival 1.00 <0.001 <0.001 <0.001 0.02 0.19 0.68 0.03
FOLR2 0.80 1.00 <0.001 <0.001 <0.001 0.48 0.03 0.16
CD163 0.63 0.53 1.00 <0.001 <0.001 0.23 0.58 0.21
CD14 0.59 0.66 0.56 1.00 <0.001 <0.001 0.13 0.13
CD206 0.32 0.47 0.47 0.43 1.00 0.40 0.18 0.84
CD16 0.18 0.10 0.31 0.44 0.12 1.00 <0.001 0.34
CD64 -0.06 -0.34 -0.09 -0.24 -0.21 0.52 1.00 0.99
CD86 -0.32 -0.21 -0.19 -0.23 -0.03 -0.15 0.01 1.00
expression on NLCs


A
CLL PBMC
NLCs
Lymphoid cells
SSC-A
FSC-A
NLCs
FOLR2
CD163
CD206
Lymphoid cells
CD14
B
positive lymphocytes [%]
0.0028
0.0005
0.0003
FOLR2
CD14
CD163
CD206
C
CLL alone (DAY0)
CLL cells
99.6%
CD5
FOLR2
0.07%
CLL PBMC (DAY12)
91.6%
7.73%
CD19
D
RNP FOLR2 electroporation
HD-monocyte (day 0)
CSF-1 activation (6 days)
freshly purified CLL cells (day 0)
heterologous co-culture (6 days)
CSF1 MDM
FOLR2 KO NLC
E
+ CTRL HD-NLCs
3.14%
+ FOLR2 KO HD-NLCs
0.03%
0.0010
FOLR2+ CLL cells [%]
+CTRL HD-NLCs
+FOLR2 KO HD-NLCs


A
CD5+/CD19+ (CA - CLL cells alone)
PKH67
CD5+/CD19+ (CC - CLL cells + NLCs)
22.4%
3.12%
0.15%
0%
FOLR2
CD14
CD16
Positive CLL cells [%]
0.0031
0.0194
PKH67
FOLR2
CD14
CD16
B
CLL cells interacting with NLC
CLL cells post-interaction
8µm
2µm
CD19FOLR2
C
Transwell co-cultures
FOLR2⁺ CLL cells [%]
0.0597
0.0606
0.0771
0.0131
0.0106
0.0342
24h
72h
CC
CA
TSW_MDM
TSW_NLC
D
Pharmacological inhibition
FOLR2⁺ CLL cells (% of control)
0.0221
0.0001
<0.0001
CC_DMSO
CA_DMSO
CC_CytoD_2µM
CC_GW4869_5µM
E
CTRL HD-NLCs co-cultures (CC)
FOLR2 KO HD-NLCs co-cultures (CC)
5µm
FOLR2 CD19 Folic acid
F
CTRL HD-NLCs CC
FOLR2 KO HD-NLCs CC
10µm
Bright field Folic acid


A
frozen CLL PBMC
HD-monocyte plating
negative selection
CSF-1 activation (Day -10)
freshly isol. CLL cells (Day -4)
CSF-1 MDM
non-activated CLL cell
HD-NLC
activated CLL cell
media addition +CD40L (Day0)
50% media exchange
CD40L +IL-15 (Day2)
CSF-1 MDMs (Day -4)
HD-NLC co-culture (CC) (Day 0)
CLL cell analysis (Day 7)
B
CLL cells
CD23
CD58
FOLR2
CD49d
CD184
CLL alone (CA)
+HD-NLCs (CC)
C
FOLR2+ CLL cells [%]
<0.0001
CC_NA
CC_ACT
D
FOLR2+ CLL cells (% of CC)
<0.0001
<0.0001
0.0002
0.0006
0.0009
<0.0001
24h
72h
CC
CA
TSW_MDM
TSW_NLC
E
CLL cells
CD23
CD58
CD49d
CD184
FOLR2
F
ES FOLR2 [%]
p=<0.001
r=0.908
CD23+[%]
p=<0.001
r=0.889
CD58+[%]
p=<0.001
r=0.986
CD49d+[%]
p=<0.001
r=0.9221
CD184low[%]


A
Ki67+ CLL cells [%]
p<0.0001
CLL alone
+HD-NLCs
B
CLL alone
CLL cells + HD-NLCs
CD23
CD184
FOLR2
Ki67
C
ESKi67 [%]
p=<0.0001
r = 0.935
Total Ki67+ CLL [%]
D
Ki67+ CLL cells [%]
0.0004
0.0086
0.0026
FAhigh
FAlow
FAneg
CTV low CLL cells [%]
0.0079
0.0483
0.0278
E
CLL cells
FAhigh
FAlow
FAneg
P1 CTV+/Ki67-
P2 CTV+/Ki67+
P3 CTV-/Ki67+
P4 CTV-/Ki67-
CTV
CD23
CD184
FOLR2
F
CLL cells
P3 CTV-/Ki67+
G5 G4 G3 G2 G1
CTV+Ki67-
CTV+Ki67+
CTV-Ki67+ G1
G2
G3
G4
G5
CTV-Ki67-
321
924
762
718
674
633
615
345
FOLR2 [MFI]


A
Reactive tonsil
#191 - classical CLL
#182 - accelerated CLL
#193 - CLL with RT
200µm
20µm
CD20 FOLR2 CD163
B
FOLR2 co-expression by CD163+ MΦ [%]
0.0485
0.0083
>0.99
100
80
60
40
20
0
Classical
Accelerated
RT
C
#190
#183
#193
5 µm
DAPI CD163 FOLR2 CD20 Ki67
D
#190
#183
#193
10 µm
DAPI CD163 FOLR2 CD20 Ki67
E
#187
#193
100 µm
FOLR2 Ki67 CD20
0.0221
FOLR2+ MΦ [%]
25
20
15
10
5
0
<25% Ki67+
>25% Ki67+

Supplement

Supplementary methods:

Cell isolation

Peripheral Blood Mononuclear Cells (PBMC) were isolated from blood of CLL patients or HD buffy coats by density-gradient centrifugation, and used directly for the downstream processing or cryopreserved using CryoStor CS10 (STEMCELL).

CLL cells were purified from PBMC, using a EasySep™ Human B Cell Enrichment Kit II Without CD43 Depletion negative selection kit (STEMcell, France), according to manufacturer's protocol. CLL cells used for heterologous co-cultures were purified from cryopreserved PBMC. To minimize cell death, PBMC were thawed the day before purification, and cultured in appropriate media at 10×10^6 c/mL. For experiments measuring cancer cell proliferation, right after purification, CLL cells were stained with CellTrace™ Violet (CTV; Invitrogen) according to manufacturer instructions. Cell purity and viability were evaluated by flow cytometry using CD5 and CD19 antibodies and viability staining, and consistently exceeded 95% across all samples (data not shown).

Healthy donor monocytes were purified using CD14 MicroBeads positive selection kit and MS/LS columns (Miltenyi Biotec, France), according to the manufacturer's protocol. Isolation efficacy was evaluated by flow cytometric analysis of $CD14^+$ cell frequency, and exceeded 95% (data not shown). Freshly isolated monocytes were used to generate monocyte-derived macrophages (MDMs) or healthy donor NLCs (HD-NLCs).

Cell cultures

In vitro cultures were conducted in complete medium, composed of RPMI 1640 with GlutaMAX (Gibco, France), supplemented with 10% fetal bovine serum (FBS, Life Technologies, France) and 100 µg/ml of penicillin/streptomycin (Sigma-Aldrich, France). For experiments with varying concentration of folic acid (FA), media were prepared on the basis of RPMI 1640 without folic acid (Gibco, France) and 100 µg/ml of penicillin/streptomycin. For FA^{high} condition, the media was supplemented with standard 2.27µM FA concentration. Subsequently, both FA^{high} and FA^{low} media were supplemented with 10% FBS. For $FA^{negative}$ condition, 10% of dialyzed FBS (Sigma, Germany) was used instead.

Cells were plated in tissue culture-treated plates (Corning, USA) at varying volumes: 4 mL per well for 6-well plates, 1.5 mL per well for 12-well plates, and 500 µl per well for 48-well plates. All cultures were maintained at 37°C in a humidified atmosphere with 5% CO2.

Autologous nurse-like cells (NLCs) were generated by the culture of freshly isolated CLL PBMC at 10×10^6 cells/mL in complete medium for up to 15 days[1]. For NLCs phenotyping, combined fractions of floating cells collected by pipetting, and adherent cells detached by Accutase were used.

Monocyte-derived macrophages (MDMs) were generated by activating purified $CD14^+$ monocytes with either 20 ng/mL CSF-1 or 50 ng/mL GM-CSF during 6 days for initial differentiation of M2-like or M1-like MDMs, respectively. Subsequently, cells were polarized for 48 hours with 25 ng/mL IL-4 and 25 ng/mL IL-13 to generate M2-like MDMs, or with 100 U/mL IFNγ and 10 ng/mL LPS to generate M1-like MDMs.

Heterologous co-culture system

A heterologous co-culture system combining purified monocytes from healthy donors (HD) and CLL cells from patient blood was used for generation of HD-NLCs, and studying FOLR2 trogocytosis in conditions mimicking lymph node microenvironment.

Basic protocol (fig. S4A): $CD14^+$ healthy donor monocytes were plated at 0.5×10^6 cells/mL in a 48-well plate and cultured in 500 µL of complete medium (CM) supplemented with 20 ng/mL CSF1. After 6 days, co-culture was

initiated by removing the spent medium and adding purified naïve CLL cells at 10×10^6 cells/mL in 500 µL of fresh CM. After 5 days of co-culture, cells were activated with either 10 ng/mL IL-2 and 1 µg/mL CpG, or 50 ng/mL CD40L and 10 ng/mL IL-15, for 72 hours.

Optimized protocol (fig. 4A): MDMs were generated by plating $CD14^+$ cells at 1×10^6 cells/mL in 250 µL of CM supplemented with 20 ng/mL CSF-1, in a 48-well plate. After 6 days, medium was replaced and purified naïve CLL cells were added at 6×10^6 cells/mL in 250 µL of CM, to initiate the co-cultures. 4 days later, after polarization of HD-NLC, 250 µL of fresh medium containing CD40L was added to a final concentration of 25 ng/mL. 2 days later, 300 µL of medium was replaced, and cells were further stimulated with 50 ng/mL CD40L and 10 ng/mL IL-15 for 5 days.

Transwell cultures

CLL cells were seeded in the lower compartment of Transwell plates, whereas MDMs or NLCs were placed in the upper insert. MDMs were generated by CSF-1 stimulation for 6 days, transferred to Transwell inserts, and allowed to adhere overnight. The following day, CTV-labeled CLL cells were added to the lower compartment. For NLC conditions, unstained CLL cells were first added to MDMs to promote NLC differentiation before transfer to the insert and were maintained together with the macrophages throughout the Transwell culture. FOLR2 acquisition and CLL cell viability were assessed by flow cytometry after 24 and 72 h.

Pharmacological perturbations

Mature CSF-1-derived MDMs and purified CLL cells were separately pretreated for 30 min with cytochalasin D (2 µM), an inhibitor of actin polymerization, or GW4869 (5 µM), an inhibitor of neutral sphingomyelinase commonly used to suppress ceramide-dependent extracellular vesicle biogenesis, before initiation of co-culture. Cells were subsequently combined and cultured in the continued presence of the respective compounds; DMSO-treated cultures served as vehicle controls. FOLR2 acquisition and CLL cell viability were assessed by flow cytometry after 24 h.

Flow cytometry

Extracellular staining: All tested samples were re-suspended in the staining buffer (5% FBS, 0,5% BSA, 2mM EDTA, 0.1% sodium azide in PBS), supplemented with 2.5 µg/mL Human BD Fc Block™ (BD Pharmingen, France) and 1% human serum to prevent the non-specific antibody binding, and incubated for 15 min at 4°C. Subsequently, cells were stained with antibodies at saturating concentrations, for 20 min at 4°C. After washing, cells were re-suspended in PBS, containing 0.8 µg/mL 7-AAD (Sony, USA).

Intracellular staining: Cells were stained with FVS620 viability dye (BD) or Zombie NIR (Thermo Fisher Scientific) according to manufacturer's protocol. Following the extracellular staining, cells were fixed and permeabilized with True-Nuclear™ Transcription Factor Buffer Set (Biolegened). Next, cells were stained with anti-Ki67 mAb (Invitrogen) for 20 min at RT, washed and re-suspended in PBS.

AnnexinV/7-AAD staining of CLL cells: Cells were washed and resuspended in Annexin-V buffer and stained with Annexin-V-FITC (Miltenyi, Germany) according to manufacturer protocol. Afterward, cells were resuspended in Annexin-V buffer containing 0.8 µg/mL 7-AAD.

Results: were analyzed using FlowLogic 7.00.2 software (Inivai Technologies). Gating strategies for the analysis of CLL cell activation and proliferation are provided in the Supplementary Information (Fig. S4E and S5A, respectively). Gates for $FOLR2^+$ cells were set using fluorescence-minus-one (FMO) controls.

The analysis of the enrichment of $FOLR2^+$ trogocytic cells in the population of activated CLL cells, was made by introducing a FOLR2 enrichment score (ES_{FOLR2}), further correlated with the total percentage of CLL cells positive for a specific activation marker (Fig. S4F; A). Ki67 enrichment score was calculated analogously, to represent enrichment of $Ki67^+$ CLL cells in the population of $FOLR2^+$ trogocytic CLL cells.

Gene expression analysis with quantitative RT-PCR

To evaluate FOLR2 gene expression, cell pellets stored in -80°C, were resuspended in TRIzol™ Reagent, and RNA was isolated using Direct-zolTM RNA MiniPrep kit according to manufacturer instruction. Subsequently, reverse transcription was performed on purified RNA using SuperScript™ III enzyme, and complement DNA was amplified by polymerase chain reaction (PCR). Primers targeting FOLR2 gene were based on[2], and validated using M2-like MDMs and FOLR2 KO M2-like MDMs as positive and negative controls respectively, prior to application in CLL samples. Quantitative PCR using PowerUp™ SYBR™ Green Master Mix, was performed on StepOnePlus Real-Time PCR Systems (Applied Biosystem), using standard protocol with Tm = 60°C and 40 amplification cycles. FOLR2 gene expression was calculated using the comparative $2^{-}\Delta\Delta Ct$ method, normalizing the results with GADPH housekeeping gene.

FOLR2 gene knockout using RNP Crispr-Cas9 method

Freshly isolated $CD14^{+}$ monocytes from a healthy donor were activated with 20 ng/mL CSF-1, and seeded in CM without antibiotic for 16h. CrRNA and tracrRNA were reconstituted in Nuclease Free Duplex Buffer (IDT, USA), and mixed in equimolar concentrations, followed by heating at 95°C for 5 min. Each gRNA was combined with Alt-R™ S.p. HiFi Cas9 Nuclease V3 at a 1:1.2 molar ratio, incubated at 37°C for 15-20 min, and cooled down to RT. After detachment, monocytes were resuspended in buffer T (Neon™ Transfection System 100 µL Kit), mixed with RNP complexes, and electroporated in Neon Tip with Neon Transfection System, at 1900V, 20ms, single pulse. Afterwards, cells were plated in antibiotic free medium with 25 ng/mL CSF-1, and cultured for 5 days to allow maturation of MDMs. After confirmation of FOLR2 gene knockout (KO) effectiveness by qPCR (Fig. S2B) or flow cytometry (Fig. S2D), naïve purified CLL cells were mixed with FOLR2 KO MDMs to induce polarization of HD-NLCs and facilitate cell-cell interactions. After 6 days, CLL cells were analyzed by flow cytometry.

Immunofluorescence of *in vitro* cells

Following the long-term *in vitro* culture (12-14 days), CLL PBMC were harvested and re-suspended in the staining buffer (5% FBS + 0.5% BSA + 1mM EDTA in PBS) containing 1% human serum and 2.5 µg/mL Human BD Fc Block™ (BD Biosciences, France) and incubated for 15 min at 4°C. For detection of extracellular antigens, cells were first stained indirectly with rabbit anti-FOLR2 mAbs (Abcam) for 20 min at 4°C, followed by washing wish PBS, and incubation with goat anti-rabbit IgG secondary antibodies conjugated with AF647 (Invitrogen) for 15 min at 4°C. Next, cells were incubated with mouse anti-CD19 antibody conjugated with BV421 (Sony) for 20 min at 4°C. Subsequently, cells were washed four times with PBS and fixed with 4% PFA in PBS for 20 min at RT. After three washes with PBS, cells were counterstained with DAPI (1µg/mL) for 5 min, washed twice with PBS and left on the cover glass O/N at 4°C to facilitate attachment of the cells. The next day, slides were mounted using Fluoromount media (Thermo Fisher Scientific), and imaged using confocal microscope LSM 780 or 880 (Zeiss). Images were analyzed using ZEN blue 3.12 software (Zeiss).

Immunohistochemistry of Patient Tissue Samples

Multiplex Immunofluorescence (mIF): the BOND RX staining platform (LEICA Biosystems, Germany) was used to automate the mIF staining procedure on 4 µm FFPE tissue sections. After baking and dewaxing, tissue slides were heat-pretreated for 20 min at 100°C using ER2 pretreatment solution (pH9, LEICA Biosystems, Germany). The slides were blocked for endogenous peroxidase activity using the Discovery inhibitor (15 minutes at room temperature) (07017944001, Roche Diagnostics, Switzerland). The slides were then stained for 5-plex immunofluorescence using the OPAL™ Technology (AKOYA Biosciences, USA) with sequential denaturation using ER1 pretreatment buffer (pH6, LEICA Biosystems, Germany), for 20 min at 97°C between each antibody-staining cycle. Primary antibodies were applied and incubated during 30 min at room temperature programmed in the aforementioned staining cycles in the following order: FOLR2 (clone EPR25731-70 (ABCAM Netherlands), at final dilution of 1/200, Envision Flex antibody diluent, Agilent Technologies), Ki67 (clone SP6, Ready to use, Zytomed, by Diagomics, France), CD163 (clone MRQ-26, Ready to use, Roche Diagnostics), CD68 (clone PGM-1, at dilution of 1/100, in Envision Flex antibody diluent) and CD20 (clone L26, Ready to use antibody diluted at ¼ in Ventana

Antibody diluent, Roche Diagnostics). Subsequently, slides were incubated using the Opal polymer HRP detection system, allowing for OPAL™ dye precipitation. Five OPAL™ dyes with excitation and emission wavelengths compatible with our whole slide imaging system were used: OPAL™ Polaris 480, OPAL™ 520, OPAL™ 570, OPAL™ 620 (1/300 in 1x Plus Automation Amplification Diluent, AKOYA Biosciences, USA) and OPAL™ 690 (1/150 in 1x Plus Automation Amplification Diluent). The tissue slides were counterstained using Spectral DAPI (AKOYA Biosciences, USA) and mounted with Invitrogen™ ProLong™ Gold Antifade Mounting medium (Life Technologies, USA). Whole tissue slides were scanned with ZEISS Axio Scan.Z1 microscope, using a Plan-Apochromat 20x/0.8 M27 objective in 1,1 binning mode. For visualization of trogocytosis in the tissue, selected regions were imaged with Zeiss 980 confocal microscope, using Plan-Apochromat 40×/1.3 oil objective.

Image analysis: basic image processing and analysis, including region-of-interest selection and co-localization measurements, were performed using ZEN 3.12 software (ZEISS, Germany). For signal quantification, the mIF images were initially processed with HALO software (version 3.6, Indica Labs, USA). Briefly, each section was manually annotated to include the maximal tissue area while excluding artifacts introduced during sample preparation. Subsequently, segmentation parameters were optimized to achieve the most consistent cell detection, and threshold for each marker was adjusted to minimize false-positive events. The annotated regions were then segmented, and the resulting image-analysis data were exported as FCS files for downstream analysis in Flow Logic 700.2A software (Inivai Technologies, Australia). Each cell was classified based on the combination of specific dye intensities and the completeness of its nuclear or cytoplasmic region. Results were analyzed and plotted using GraphPad Prism 10.1.2 (USA).

Statistical analysis

NLC stratification based on FOLR2 expression (Fig. 1D): FOLR2^neg (MFI <1500), FOLR2^low (MFI 1500–4500), and FOLR2^high (MFI >4500), representing low/background, intermediate, and high FOLR2 expression, respectively. The thresholds were defined independently of CLL cell viability and were used to facilitate comparison of cultures with distinct NLC FOLR2 phenotypes. In parallel, the association between FOLR2 expression and CLL cell survival was evaluated using FOLR2 MFI as a continuous variable (Fig. S1E).

Correlation between FOLR2 expression on NLCs and CLL cell survival (Fig. 1F). Because CLL cell viability displayed a non-linear distribution with a pronounced ceiling effect in cultures containing protective NLCs, samples were stratified into three ordered categories representing low (<70%), intermediate (70–85%), and high (>85%) CLL cell survival. These thresholds separated three non-overlapping regions of the observed viability distribution and represented cultures with poor, partial, and strong NLC-mediated prosurvival effects, respectively. The association between NLC marker expression and the ordered CLL cell survival categories was evaluated using Spearman rank correlation.

Choice of statistical test for transwell analyses, inhibitor experiments, and activation experiments: for transwell co-culture experiments, each experimental unit consisted of a unique combination of CLL cells from one patient and monocytes from one healthy donor. The same CLL patient–healthy donor combination was evaluated across the different culture conditions, allowing matched comparisons. Data from the 24- and 72-h time points were analyzed separately. Because some measurements were unavailable due to cell shortage or technical issues, statistical significance was assessed using a mixed-effects model with matching across conditions and Geisser–Greenhouse correction for nonsphericity, followed by Dunnett's multiple-comparisons test comparing each condition with the direct co-culture control (CC).

Supplementary tables (see Supplementary Excel Tables)

Supplementary Table S1. Key resources used in the study. List of antibodies, reagents, cell-culture materials, CRISPR reagents, equipment, and software used in the study, including supplier and identifier information where applicable.

Supplementary Table S2. Patient characteristics of CLL PBMC samples used in in vitro experiments. Clinical and biological characteristics of the patient samples included in the in vitro analyses, including available IGHV mutation status and other relevant sample information.

Supplementary Table S3. Patient characteristics of lymph-node samples analyzed by multiplex immunofluorescence. Characteristics of lymph-node samples included in the tissue analysis, including diagnostic category and available clinical information.

Supplementary Figures

Supplementary Figure S1

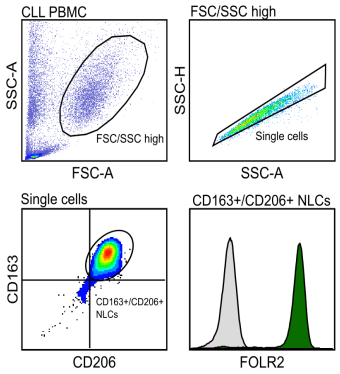


Figure S1A. Gating strategy for flow cytometric analysis of FOLR2 expression on nurse-like cells (NLCs). Grey: isotype control; dark green: anti-FOLR2.

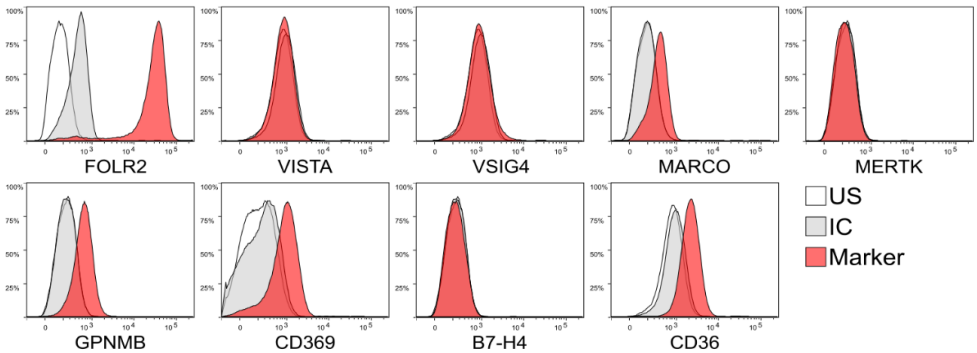


Figure S1B. Screening of novel potential marker for NLCs. NLCs were generated by high-density culture of CLL PBMC. After 14 days, cells were collected, stained with specific antibodies, and analyzed by flow cytometry. NLCs were gated based on high forward (FSC) and side scatter channel (SSC), and results for each marker were depicted by representative histogram overlay between signal from: unstained cells (US), isotype control antibody (IC), and antibody against antigen of interest (Marker).

Rationale for selecting macrophage surface markers for screening: VISTA (V-domain Ig suppressor of T-cell activation) was selected based on its expression by tumor-associated myeloid cells in acute myeloid leukemia (Correia da Cruz L et al. 2025, Biomedicine & Pharmacotherapy 189:118287); VSIG4 (V-set and immunoglobulin domain-containing 4) as a marker associated with tissue-resident macrophages (Liu B et al. 2023, Cancer Letters 553:215996); MARCO (macrophage receptor with collagenous structure) because of its reported expression by tumor-associated macrophages in acute myeloid leukemia (Li W et al. 2022, Journal of Hematology & Oncology 15:110); and MERTK (MER proto-oncogene, tyrosine kinase) as an efferocytic receptor expressed by macrophages within the acute myeloid leukemia microenvironment (Cruz Cruz J et al. 2023, Frontiers in Immunology 14:1146721). GPNMB (glycoprotein non-metastatic melanoma protein B) was included based on its expression by macrophage populations in lymph nodes from patients with follicular lymphoma (Haradhvala NJ et al. 2026, Cancer Discovery, doi:10.1158/2159-8290); CD369/Dectin-1 (CLEC7A) because of its association with immunoregulatory myeloid cells, including MDSCs (Nakano S et al. 2022, Biological & Pharmaceutical Bulletin 45:1053–1060); B7-H4 as an immune-checkpoint molecule expressed by tumor-associated macrophages (Hu X et al. 2020, Neoplasia 22:539–553); and CD36 as a multifunctional scavenger receptor and long-chain fatty-acid transporter highly expressed by tumor-associated macrophages (Albakri MM et al. 2022, Journal of Leukocyte Biology 112:617–628).

These markers were therefore selected as candidate indicators of protumoral, immunoregulatory, tissue-resident, efferocytic, or metabolically adapted macrophage states, with the aim of identifying phenotypic features that could further distinguish protective NLCs. Among the tested markers, FOLR2 showed a particularly strong expression and connection with protective NLC phenotype, and was therefore selected for further functional investigation.

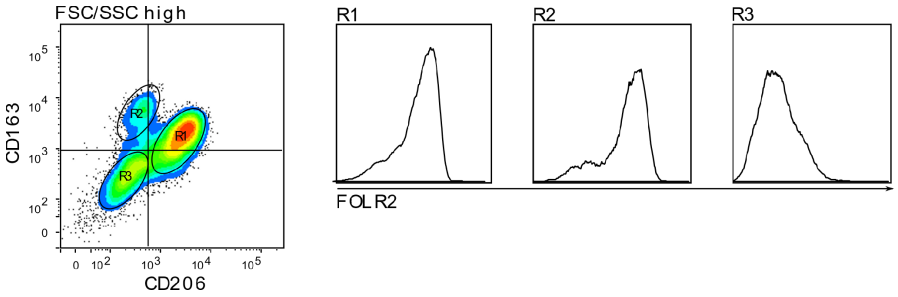


Figure S1C. Detection of heterogeneous subpopulations of NLCs with varying expression of FOLR2. NLCs generated *in vitro* were analyzed by flow cytometry. An exemplary dot plot shows NLCs, divided into three subpopulations (R1-R3), based on the expression of typical macrophage's markers: CD163 and CD206.

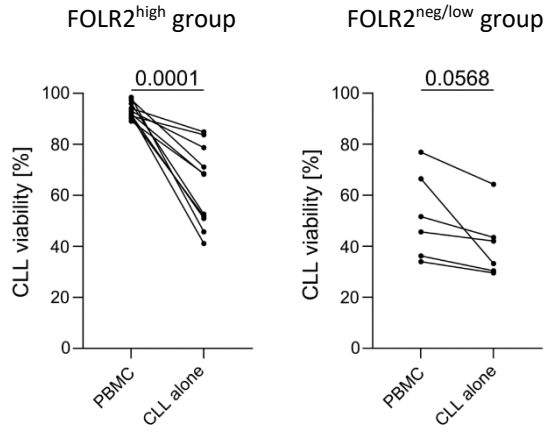


Figure S1D. Presence of FOLR2^{high} NLCs is associated with increased survival of CLL cells *in vitro*. For a subset of the patient samples described in Fig. 1F-G, in addition to PBMC cultures (which allow for the outgrowth of NLCs), a fraction of leukemic cells was purified by negative selection and cultured at the corresponding density of 10 × 10^6 cells/mL (CLL alone). CLL cell viability was assessed by Annexin V/7-AAD staining on days 12–14 for PBMC cultures and on day 7 for CLL cultured alone. Paired PBMC-CLL alone samples from the same patient were divided into two groups (FOLR2^{high} with n = 11 samples, and FOLR2$^{neg/low}$ with n = 6 samples), based on FOLR2 expression on NLCs (according to Fig. 1D). Survival of CLL cells between the two culture conditions was compared using a paired, two-tailed t-test, with P values < 0.05 considered statistically significant.

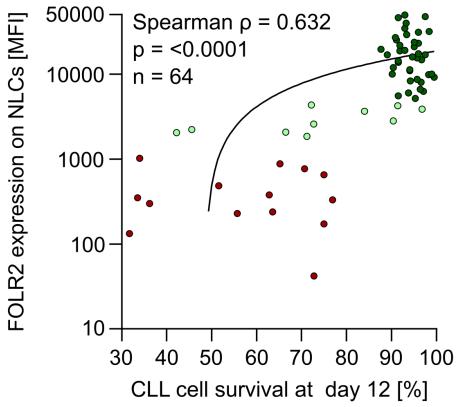


Figure S1E. FOLR2 expression by NLCs is positively associated with CLL cell survival during PBMC culture in vitro. Correlation between FOLR2 expression by NLCs and CLL cell viability measured on days 12–14 of PBMC culture in n = 64 patient samples. Color codes correspond to sample groups defined based on FOLR2 expression by NLCs (Fig. 1D). The association was assessed using Spearman correlation. P values < 0.05 were considered statistically significant.

Supplementary Figure S2

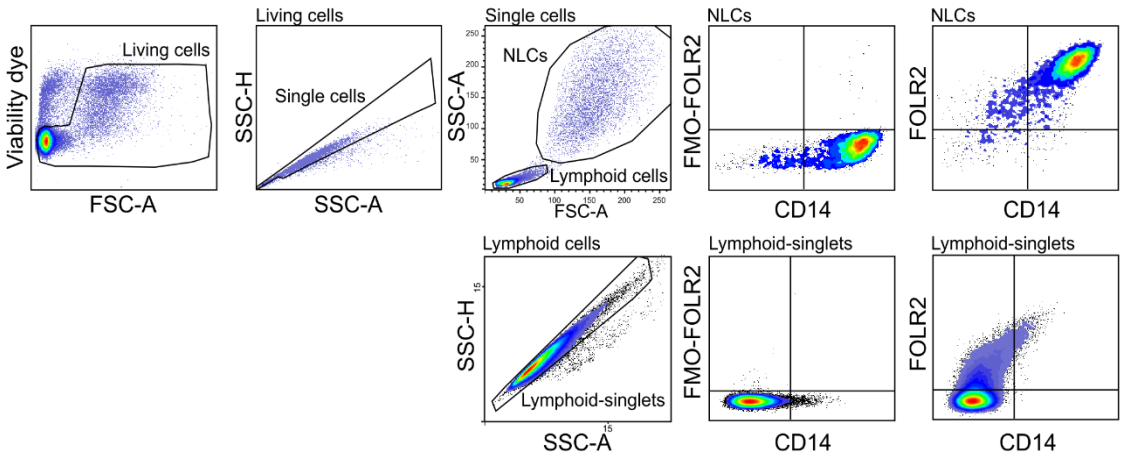


Figure S2A. Gating strategy for flow cytometric measurements of FOLR2 signals on NLCs and lymphoid cells. Dead cells were excluded based on 7-AAD staining, with gating adjusted to account for the high autofluorescence of NLCs. Cell doublets were excluded using forward-scatter (FSC; not shown) and side-scatter (SSC) parameters. PBMCs were then separated into NLCs and lymphoid cell populations based on differences in forward scatter (FSC) and side scatter (SSC). The FOLR2-positive gate was defined using the corresponding fluorescence-minus-one (FMO) control.

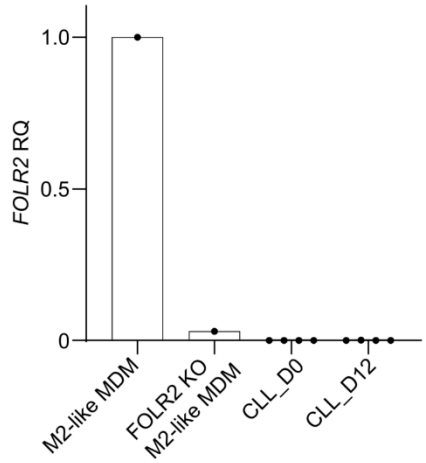


Figure S2B. CLL cells do not express the *FOLR2* gene. Freshly isolated CLL PBMCs were divided into two parts: 1) used to purify CLL cells by negative selection, followed by freezing the leukemic cells in −80°C (CLL_D0); 2) was cultured *in vitro* for 12 days to allow NLC outgrowth, after which CLL cells were purified by negative selection and frozen at −80°C (CLL_D12). After collecting all the samples, *FOLR2* gene expression in CLL cells was measured by qPCR, using M2-like MDMs and *FOLR2* KO M2-like MDMs as positive and negative control respectively. The graph displays pooled data from n = 4 independent experiments and four different patient samples, and M2-like MDM controls from a single healthy donor. Results of the analysis were represented as Relative Quantification (RQ) according to *FOLR2* expression by M2-like MDMs.

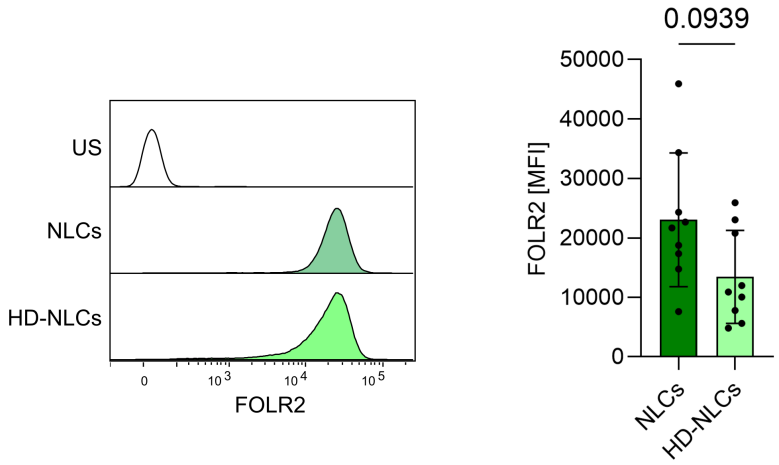


Figure S2C. HD-NLCs express comparable levels of FOLR2 to autologous NLCs. Flow cytometric analysis of FOLR2 expression on NLCs generated in standard autologous CLL PBMC cultures (dark green) and healthy donor-derived NLCs (HD-NLCs; light green) generated by heterologous co-culture of healthy donor CD14^{+} monocytes with purified CLL cells. US, unstained NLC control. **Left)** representative histogram overlay. **Right)** quantification of FOLR2 expression on autologous NLCs generated from PBMC samples of 9 CLL patients and on HD-NLCs generated by co-culture of purified CLL cells from 9 patients with monocytes from 9 healthy donors. Bars represent mean ± SD. HD-NLCs showed a trend toward lower FOLR2 expression than autologous NLCs, but the difference was not statistically significant by Mann–Whitney U-test.

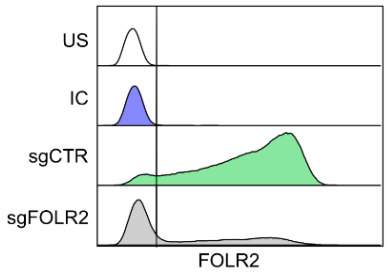


Figure S2D. Downregulation of FOLR2 protein expression in MDMs following *FOLR2* knock-out. CD14^{+} monocytes from healthy-donor PBMC were isolated by positive selection, and activated with CSF1 for 16h. Subsequently, the monocytes were electroporated with sgRNA targeting FOLR2 with RNP Crispr-Cas9 approach. On day 5 after electroporation, monocyte-derived macrophages (MDMs) were collected, and FOLR2 expression was measured by flow cytometry. Results are represented as histogram overlay. US - unstained cells, IC - isotype control, sgCTR - MDMs after electroporation with a control sgRNA, sgFOLR2 – MDMs after electroporation with sgRNA targeting *FOLR2*.

Supplementary Figure S3

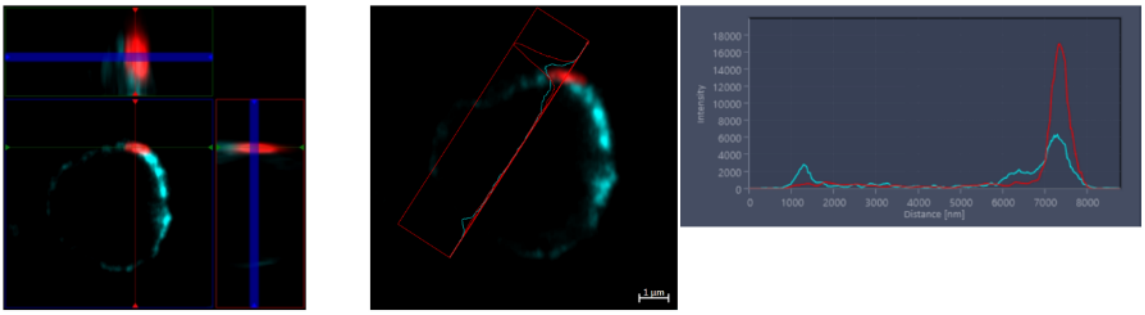


Figure S3A. FOLR2 co-localizes with CD19 in the plasma membrane of CLL cells. Visualization of signal co-localization between CD19 (cyan) and FOLR2 (red) in the plasma membrane of CLL cells after co-culture with NLCs. Results are presented as orthogonal projection (left) and co-localization profile (right).

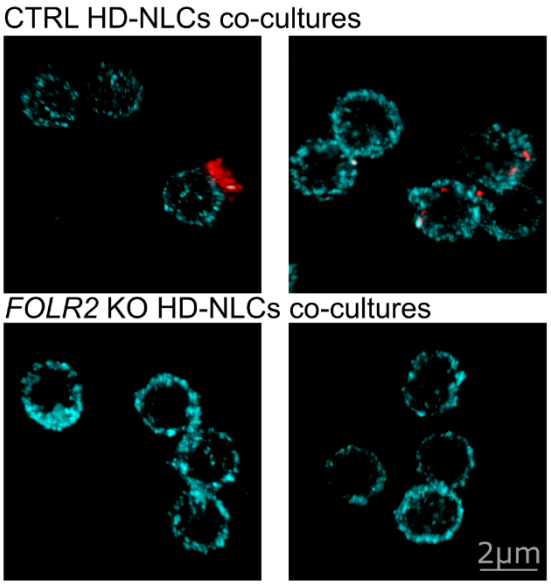


Figure S3B. Absence of FOLR2 signal on CLL cells following co-culture with FOLR2-KO HD-NLCs. Confocal microscopy images of CLL cells after co-culture with control (CTRL) HD-NLCs (upper panels) or FOLR2-KO HD-NLCs (lower panels). CD19 is shown in cyan and FOLR2 in red. Images are presented as 3D projections.

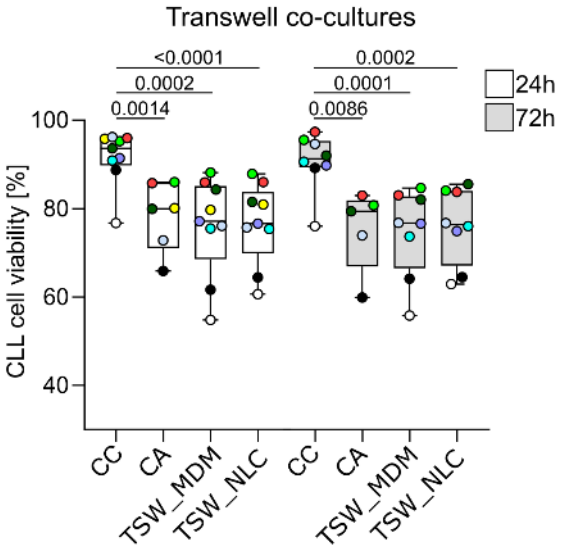


Figure S3C. CLL cell viability following transwell co-cultures. CLL cell viability was assessed by Zombie NIR staining after 24 and 72 h of culture under the same conditions as in Fig. 3C. CC – direct CLL–NLC co-culture without a transwell insert; CA – CLL cells cultured alone; TSW_MDM and TSW_NLC – CLL cells cultured in the lower compartment and physically separated by a transwell membrane from MDMs or HD-NLCs, respectively. Results from n = 3 independent experiments using CLL cells from 5 different patient samples and monocytes from 6 different healthy donors (up to 9 measurements per condition, the number of measurements varied between conditions because of technical losses). Statistical significance was assessed separately at 24 and 72h using a mixed-effects model, with matching across conditions within each unique CLL patient–healthy donor combination, followed by Dunnett's multiple-comparisons test versus CC. P values <0.05 were considered statistically significant.

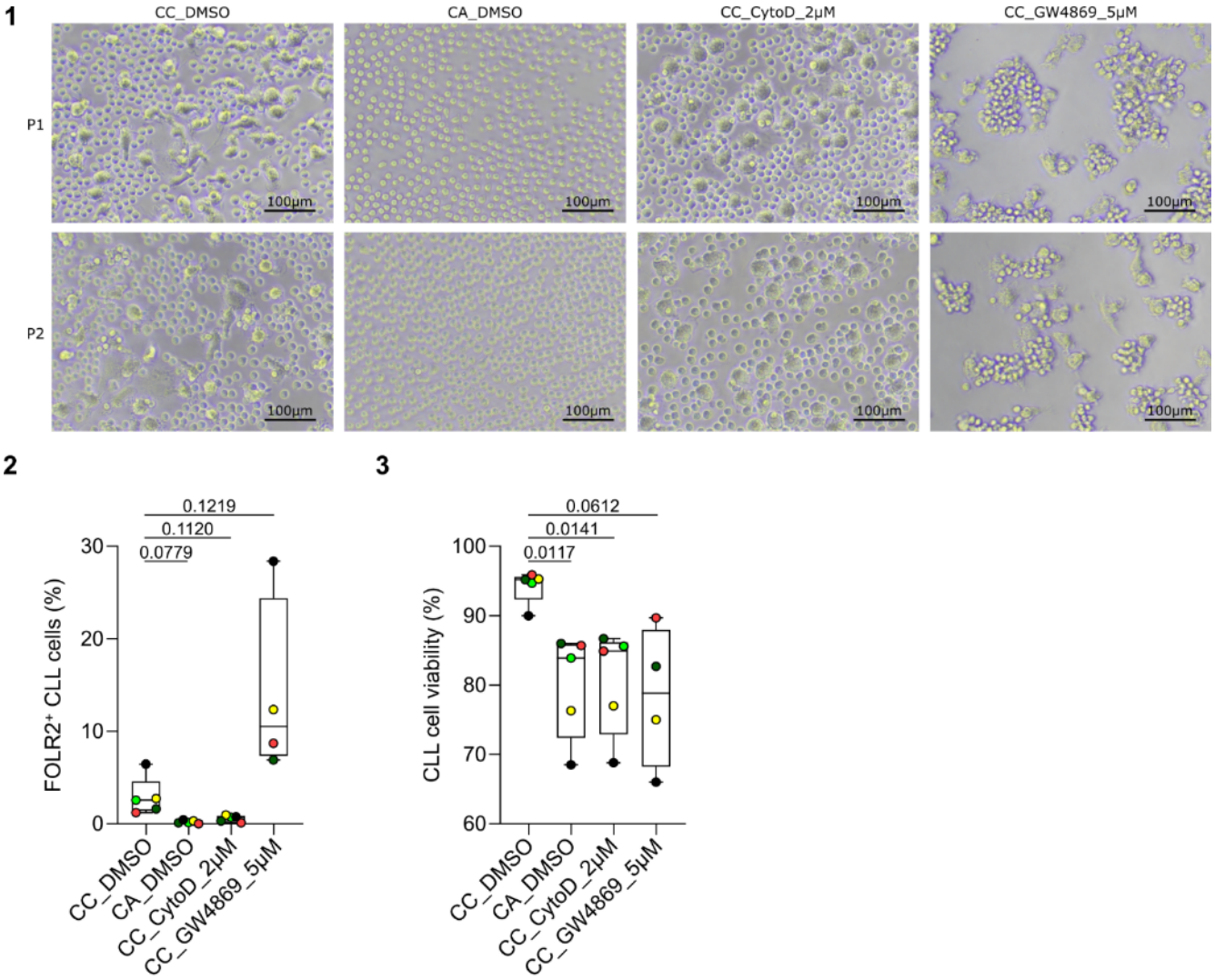


Figure S3D. Impact of cytochalasin D and GW4869 on CLL–NLC interactions, FOLR2 acquisition, and CLL cell viability. 1) Representative bright-field images of CLL–NLC co-cultures treated for 24 h with DMSO, cytochalasin D (CytoD; 2 µM), or GW4869 (5 µM), or CLL cells cultured alone (CA_DMSO). Images for two experiments, with CLL cells from two different patients, acquired with 20× objective are shown. NLCs are identified as large adherent cells, whereas CLL cells appear as small non-adherent cells. Flow cytometric analysis of **2)** Percentage of FOLR2$^+$ CLL cells, and **3)** CLL cell viability measurements under indicated culture conditions. Results from n = 3 independent experiments, using CLL cells from 4 patients, and monocytes from 4 healthy donors (5 unique CLL patient–healthy donor combinations). Statistical significance was assessed using a mixed-effects model, with matching across conditions within each unique CLL patient–healthy donor combination, followed by Dunnett's multiple-comparisons test versus CC_DMSO. P values <0.05 were considered statistically significant.

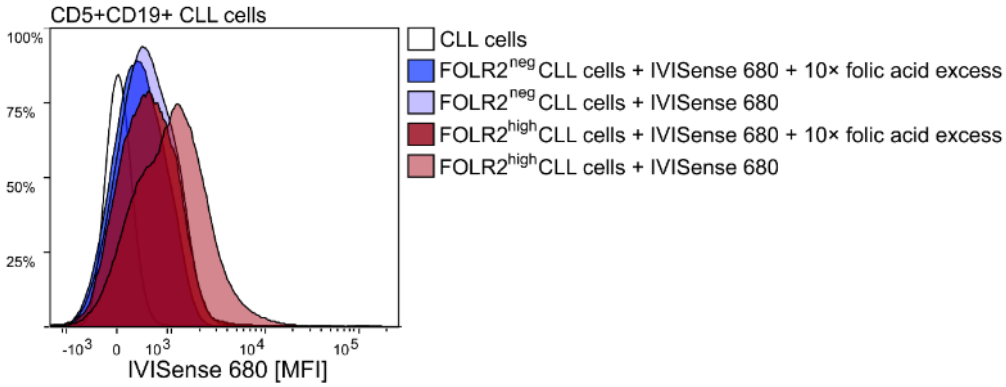


Figure S3E. FOLR2^{+} trogocytic CLL cells exhibit increased folic acid acquisition. Flow cytometric analysis of fluorescent folic acid probe (IVISense 680) acquisition by CLL cells. CLL cells following co-culture with NLCs, were re-plated and re-suspended in HBSS buffer supplemented with 5% of dFBS, and incubated with IVISense680 for 90 min, cell culture incubator at 37°C. IVISense 680 signal was analyzed, following gating on FOLR2^{neg} (blue) or FOLR2^{high} (red) subpopulation of CLL cells. As a control of IVISense680 specificity, cells were incubated with 10x excess of unlabeled folic acid. Representative results from n = 2 independent experiments.

Supplementary Figure S4

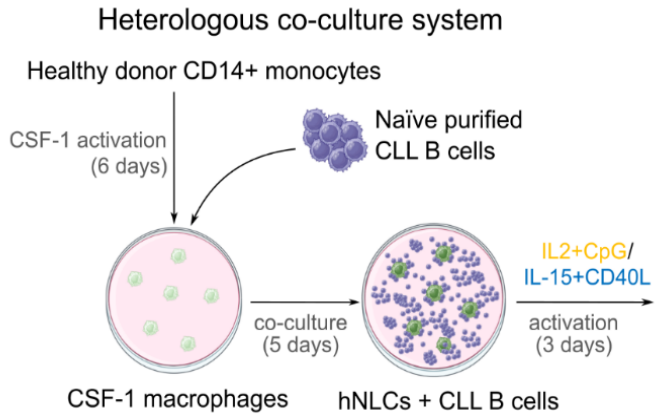


Figure S4A. Schematic of the heterologous co-culture system used to compare the effects of CD40L+IL15 and IL-2+CpG activation protocols.

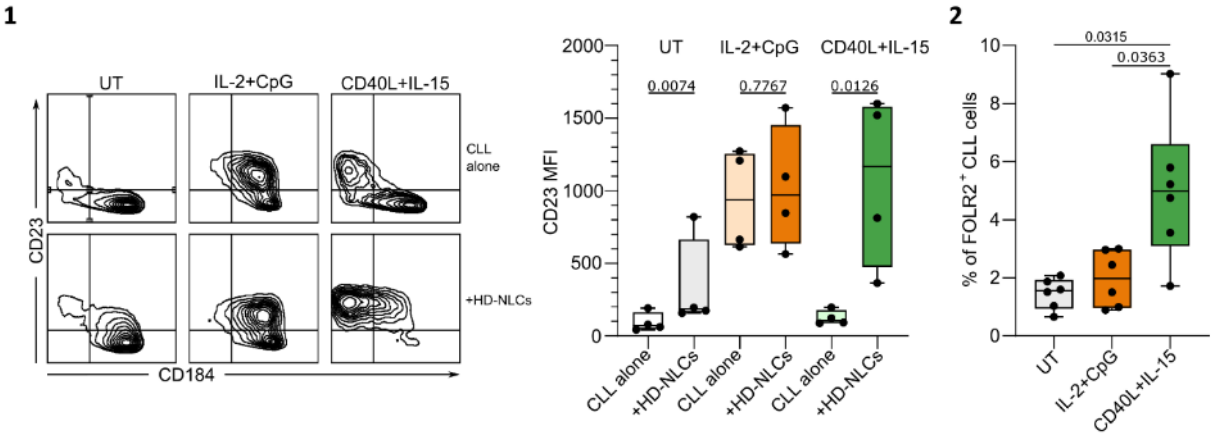


Figure S4B. CD40L+IL-15 leads to potent, NLC-dependent CLL cells activation and increased FOLR2 acquisition by leukemic cells. CLL cells were cultured alone or in a heterologous co-culture system, followed by priming with IL-2+CpG or CD40L+IL-15 for 3 days. CD23, CD184 and FOLR2 signals on CLL cells were measured by flow cytometry. 1) Representative density dot plots of CD23 and CD184 expression on CLL cells depending on activation protocol and presence of HD-NLCs; ratio paired t-test comparison of CD23 expression between CLL cultured alone or with HD-NLCs for the listed activation conditions, based on data from n = 4 different patient samples. 2) Impact of IL-2+CpG or CD40L+IL-15 treatment on FOLR2 acquisition by CLL cells in heterologous co-cultures. Data from n = 6 different patient samples was analyzed using repeated measures ANOVA with Geisser-Greenhouse correction, with P values < 0.05 considered statistically significant.

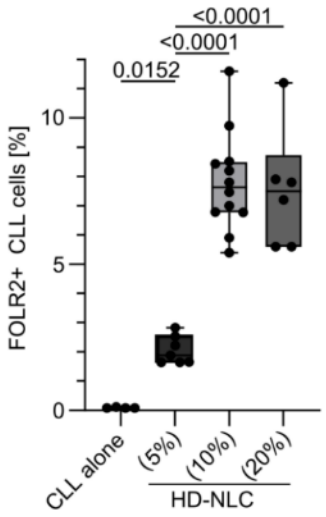


Figure S4C. Effect of HD-NLC proportion on FORL2 acquisition by CLL cells. Monocytes were plated with increasing percentage in relation to CLL cell number used for the subsequent co-cultures. After 6 days of CSF1 activation, the media was replaced, and co-cultures were initiated by addition of freshly purified CLL cells at 6 × 10^6c/mL. After 5 days of co-culture, the level of FOLR2 on CLL cells was measured by flow cytometry. Results from n = 2 independent experiments (including samples from 4 patients for CLL alone control, and 6 patients for HD-NLC groups) were analyzed by a mixed-effects model, followed by Dunnett's multiple-comparisons test , with P values < 0.05 considered statistically significant.

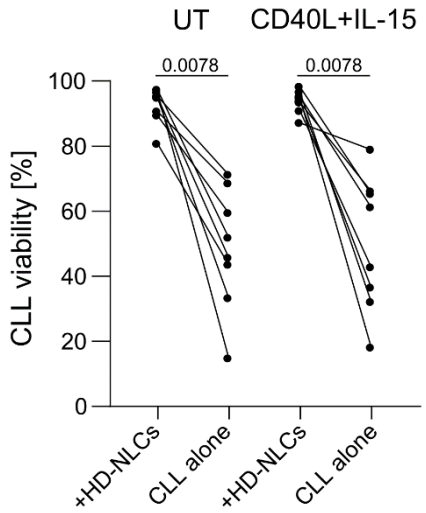


Figure S4D. HD-NLCs protect CLL cells from spontaneous apoptosis in vitro, independent of CD40L+IL-15 activation. CLL cells from heterologous co-cultures (+HD-NLCs) or monocultures (CLL alone) were treated with CD40L + IL-15 according to the optimized activation protocol. After 5 days, CLL cell viability was assessed by Annexin V/7-AAD staining (n = 1 independent experiment; samples from 8 different patients). CLL cell survival between co-cultures and monocultures, within each experimental condition were analyzed using paired, two-tailed Wilcoxon test, with P values < 0.05 considered statistically significant. UT – untreated cells.

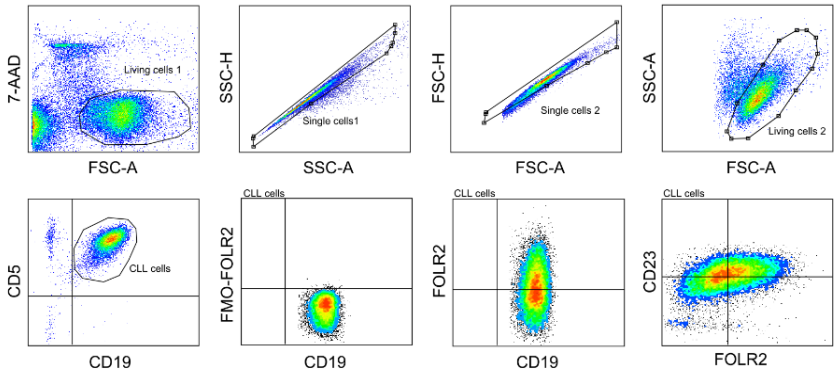


Figure S4E. Gating strategy for evaluation of CLL cell activation and FOLR2 acquisition. Dead cells were identified based on positive staining with 7-Aminoactinomycin D (7-AAD) and forward scatter (FSC). Cell doublets were excluded based on FSC and side-scatter (SSC) parameters. Remaining apoptotic/dead cells that showed not signal from 7-AAD were eliminated based on combination of FSC and SSC signals. CLL cells were gated based on positive staining with anti-CD5 and CD-19 antibodies. Positive gate for the FOLR2 signal was determined using the corresponding Fluorescence-minus-one (FMO) control.

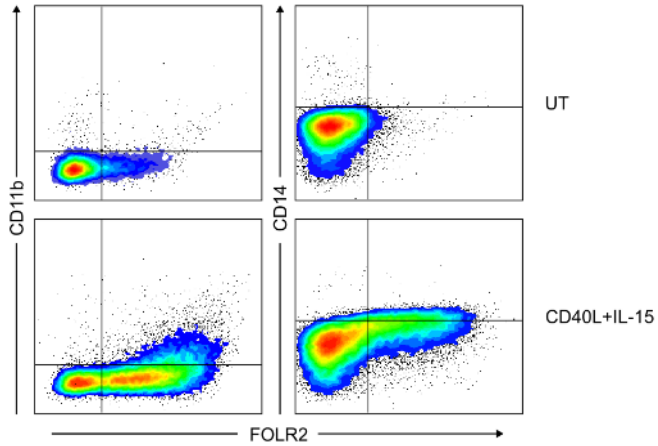


Figure S4F. CD40L+IL-15 activation intensifies trogocytosis between NLCs and CLL cells. Representative dot plots from flow cytometry analysis of FOLR2, CD11b (left, sample 1) and CD14 signals (right, sample 2) on CLL cells following co-culture with HD-NLCs, depending on CD40L+IL-15 activation. UT – untreated cells.

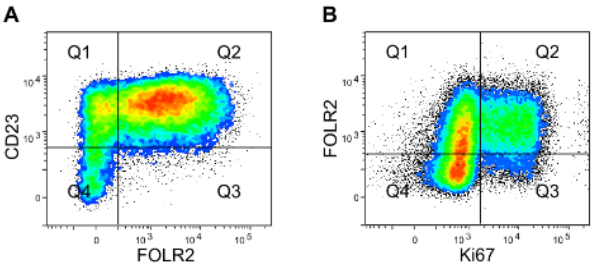


Figure S4G. Calculation of enrichment scores for evaluation of relation between FOLR2 acquisition and cell activation or proliferation.

A) Calculation of the FOLR2 enrichment scores (ES_{FOLR2}) on the example of CD23/FOLR2 staining:

ES_{FOLR2}= (Q2/Q2+Q3) × 100%

ES_{FOLR2} represents the proportion of activated cells within the FOLR2$^+$ CLL cell population. Q2 + Q3 represents all FOLR2$^+$ CLL cells, whereas Q2 represents FOLR2$^+$ cells expressing the respective activation marker (e.g., CD23 or CD58).

B) Calculation of the Ki67 enrichment score (ES_{Ki67}):

ES_{Ki67}= (Q2/Q1+Q2) × 100%

ES_{Ki67} represents the proportion of Ki67$^+$ cells within the FOLR2$^+$ CLL cell population. Q1 + Q2 represents all FOLR2$^+$ CLL cells, whereas Q2 represents FOLR2$^+$Ki67$^+$ CLL cells.

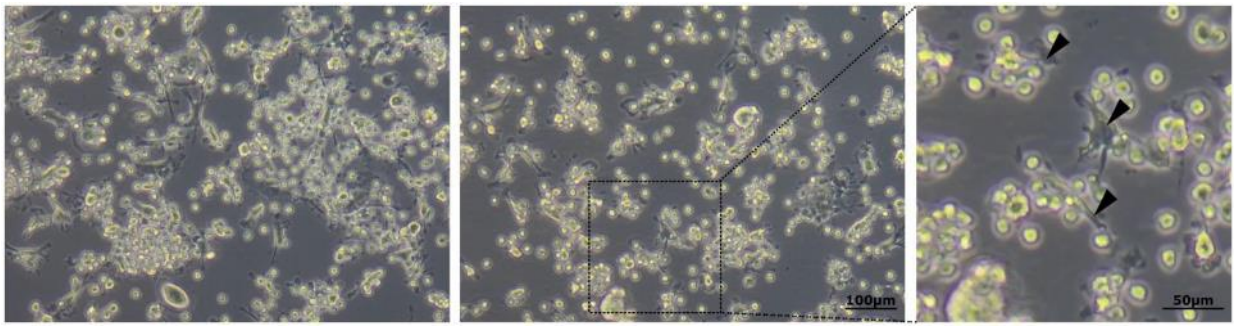


Figure S4H. Close contact between CLL cells and HD-NLCs following CD40L and IL-15 stimulation. Exemplary bright-field images of CLL and HD-NLCs co-cultures activated with CD40L and IL-15. After 96h, floating cells were gently removed by two PBS washes to visualize CLL cells remaining in close contact with HD-NLCs. The boxed region is shown at higher magnification on the right; arrowheads indicate CLL cells closely associated with HD-NLCs.

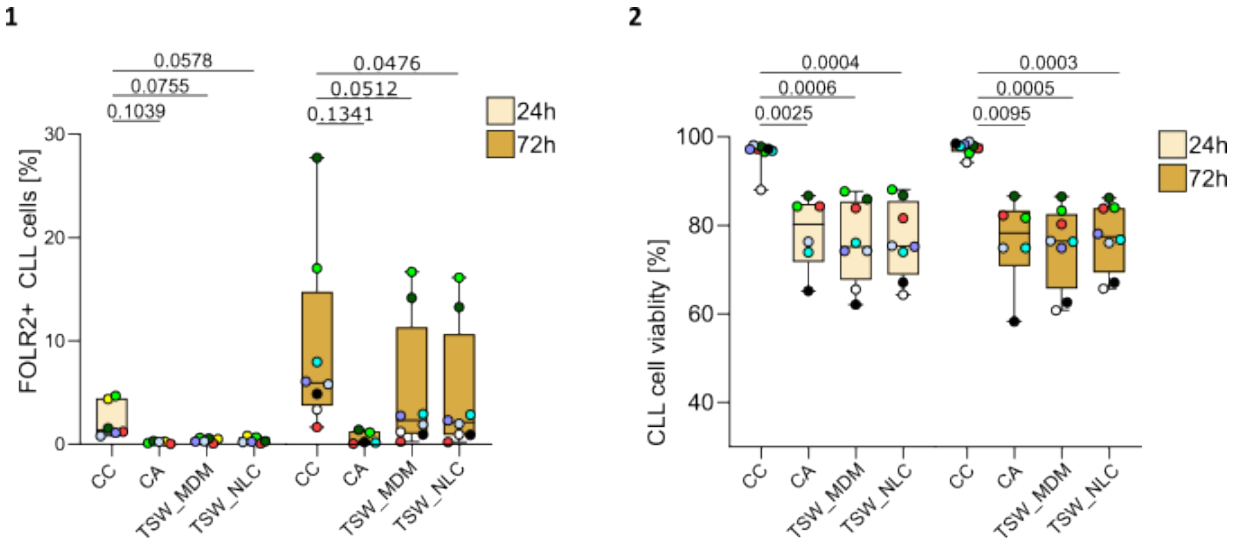


Figure S4I. Impact of physical separation from macrophages via transwell, on FOLR2 acquisition and viability of CLL cells upon CD40L + IL-15 stimulation. **1)** FOLR2 levels and **2)** CLL cell viability were measured by flow cytometry after 24 and 72 h of culture under the same conditions as in Fig. 3C. CC –

direct CLL–NLC co-culture without a transwell inserts; CA – CLL cells cultured alone; TSW_MDM and TSW_NLC – CLL cells cultured in the lower compartment and physically separated by a transwell membrane from MDMs or HD-NLCs, respectively. Results from n = 3 independent experiments using CLL cells from 5 different patient samples and monocytes from 6 different healthy donors (up to 9 measurements per condition, the number of measurements varied between conditions because of technical losses). Statistical significance was assessed separately at 24 and 72h using a mixed-effects model, with matching across conditions within each unique CLL patient–healthy donor combination, followed by Dunnett's multiple-comparisons test versus CC. P values <0.05 were considered statistically significant.

Supplementary Figure S5

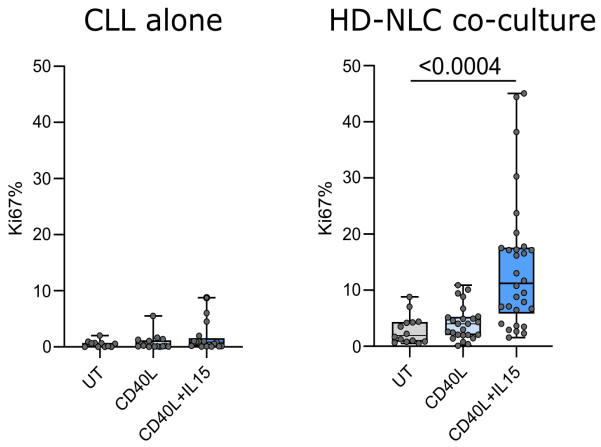


Figure S5A. IL-15 in combination with CD40L induces robust proliferation of CLL cells in the presence of HD-NLCs. Effect of CD40L (light blue) and CD40L+IL-15 (blue) activation on Ki67 expression by CLL cells cultivated alone (left) or with HD-NLCs (right) was evaluated with flow cytometry. The box-and-whisker plots display data from n = 4 independent experiments, CLL cells from 9 patients, and HD-NLCs generated from monocytes from 7 healthy donors. Repeated-measures ANOVA with Geisser-Greenhouse correction was used for data analysis, with P values < 0.05 considered statistically significant.

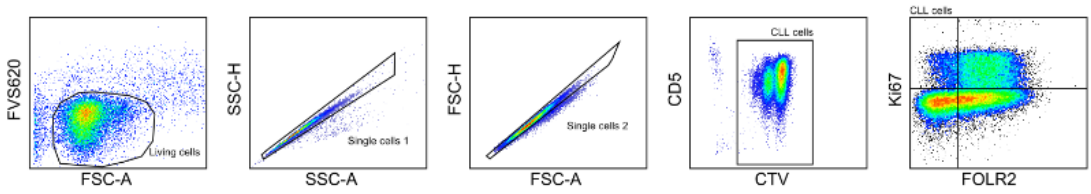


Figure S5B. Gating strategy for evaluation of CLL proliferation and FOLR2 acquisition. Dead cells were identified based on positive staining with Fixable Viability Stain 620 (FVS620) and forward scatter (FSC). Cell doublets were excluded based on FSC and side-scatter (SSC) parameters. CLL cells were gated based on positive signal of CTV and staining with anti-CD5 antibody. Positive gate for the FOLR2 and Ki67 signal was determined with isotype control antibodies.

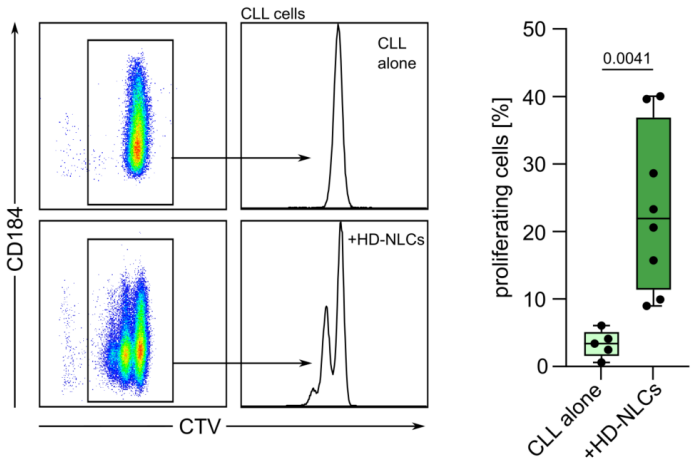


Figure S5C. CD40L+IL-15 activation leads to increased CLL proliferation in the presence of HD-NLC. Cancer cell proliferation was measured for monocultures (CLL alone) or co-cultures with HD-NLCs, 5 days after CD40L+IL-15 treatment. **Left)** Representative flow cytometry results. **Right)** Cumulative data from n = 8 patient samples showing the percentage of proliferating CLL cells based on CellTrace™ Violet (CTV) signal reduction. Results were evaluated with paired, two-tailed t-test, with P values < 0.05 considered significant.

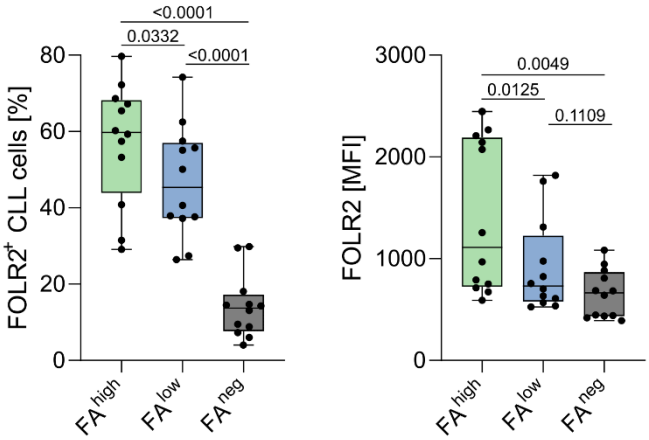


Figure S5D. Impact of folic acid availability on FOLR2 acquisition by CLL cells. CLL cells were co-cultured with HD-NLCs in the media with decreasing content of folic acid (FA): FA^{high}, FA^{low} and FA^{neg}, and analyzed by flow cytometry (n = 2 independent experiments; 8 different patient samples; 12 measurement points). Left) Comparison of $FOLR2^{+}$ CLL cell proportion, depending on FA content. Right) Comparison of FOLR2 signals on $FOLR2^{+}$ CLL cell subpopulation, depending on FA content. MFI - median fluorescence intensity. Results were analyzed by repeated-measures ANOVA with Geisser-Greenhouse correction, with P values < 0.05 considered statistically significant.

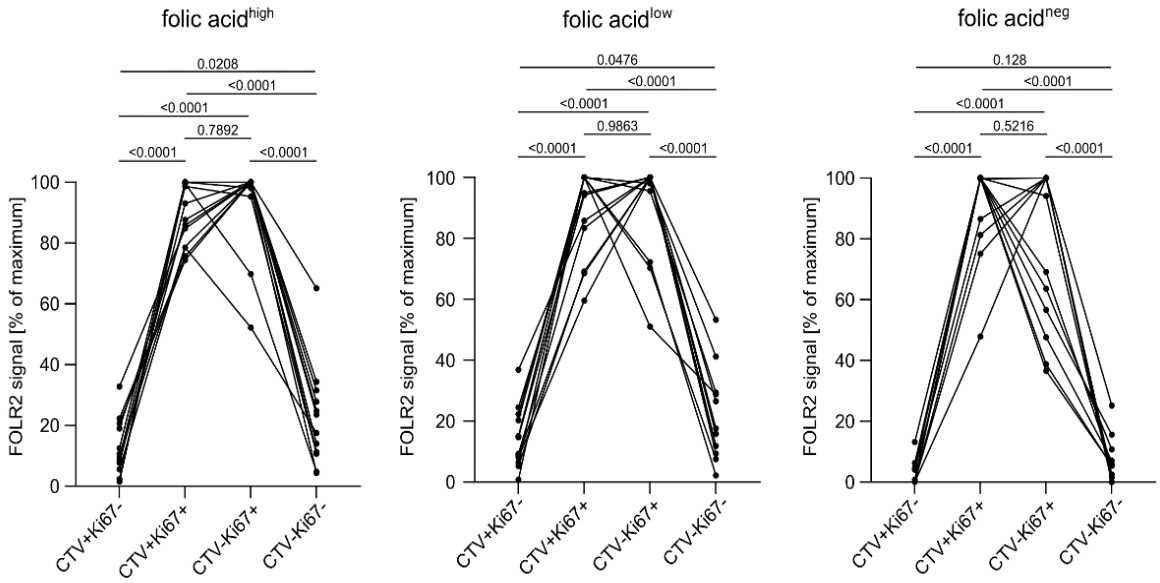


Figure S5E. FOLR2^{high}CLL cells are a subpopulation of actively proliferating leukemic cells. CLL cells were co-cultured with HD-NLCs in the media with decreasing content of folic acid (FA): FA^{high}, FA^{low} and FA^{neg}, and analyzed by flow cytometry to assess FOLR2 levels in relation to proliferative status of CLL cells. CLL cells were divided into four subpopulations (according to Fig. 5E): P1 = CTV^{high}/Ki67^{-} (quiescent, non-dividing); P2 = CTV^{high}/Ki67^{+} (right before the first division); P3 = CTV^{low}/Ki67^{+} (actively cycling, after division); P4 = CTV^{low}/Ki67^{-} (post-cycling, quiescent again). To account for heterogeneity in FOLR2 signals, FOLR2 MFI values for each patient sample and experimental condition were normalized to the highest-expressing subpopulation and presented as relative FOLR2 MFI (% of maximum). Repeated-measures ANOVA with Geisser-Greenhouse correction was used to compare FOLR2 expression by different subpopulations of CLL cells depending on their proliferation status (n = 2 independent experiments, 8 patient samples, 12 measurement points). P values < 0.05 were considered statistically significant.

Supplementary Figure S6

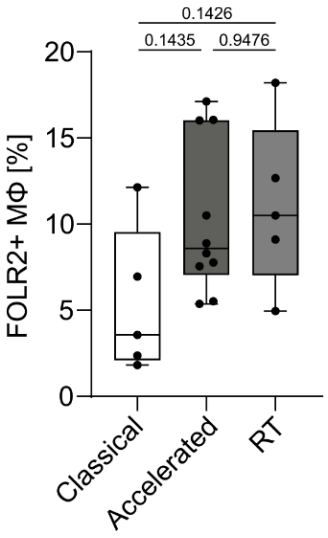


Figure S6A. Comparison of the percentage of FOLR2⁺ macrophages (MΦ) among CLL subtypes of increasing aggressiveness. Whole lymph node sections from patients with classical CLL (n = 5), accelerated CLL (n = 10) and CLL with Richter Transformation (RT, n = 5), were analyzed by multiplex immunofluorescence. Differences in the percentage of FOLR2⁺ MΦ among groups were assessed using one-way ANOVA, with P values < 0.05 considered statistically significant.

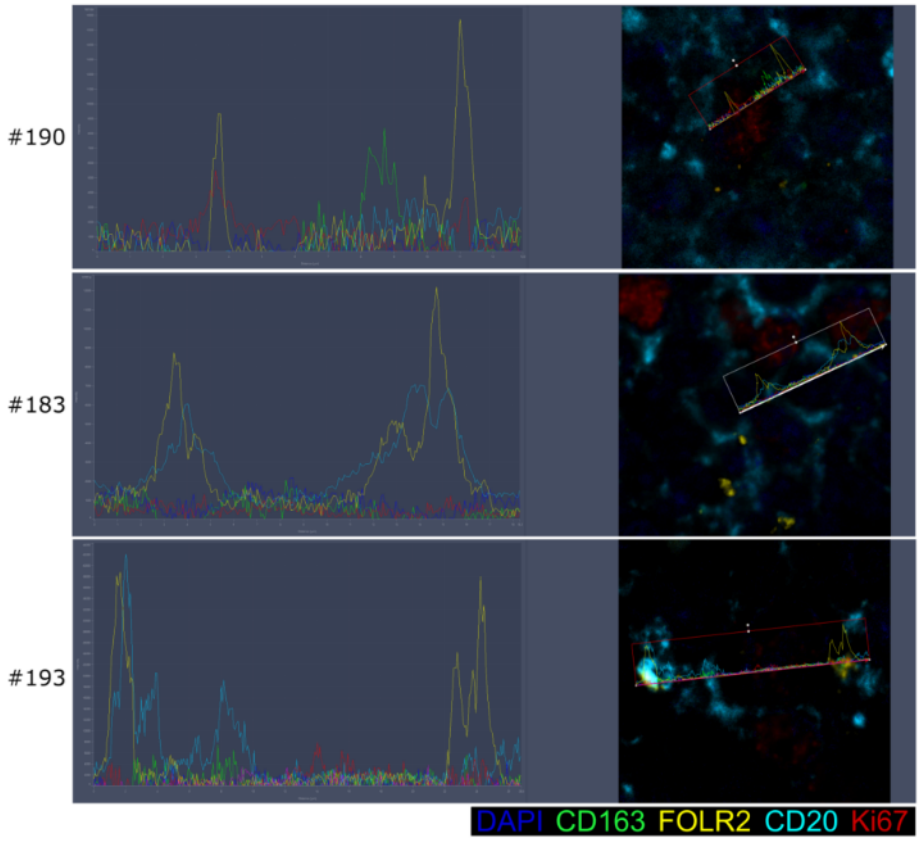


Figure S6B. Visualization of FOLR2^{+} leukemic cells in patient lymph nodes. To detect FOLR2^{+} leukemic cells *in situ*, lymph nodes from patients #190, #183, and #193 were imaged using a Zeiss 980 confocal microscope (Plan-Apochromat 40×/1.3 oil objective), focusing on regions devoid of MΦ. Subsequently, overlap between FOLR2 (yellow) signals and CD20^{+} (cyan) plasma membrane of leukemic cells or their intracellular region, was visualized by co-localization profiles of the selected z-stack sections (left), as indicated with white arrows on the corresponding image (right).